Comparative study of colon cancer subclones uncovers potential roles for AKAP7 and TP53RK in the antiviral response.

Colin Davis

A thesis submitted to the
Faculty of Graduate and Postdoctoral Studies
in partial fulfillment of the requirements for the
MSc degree in Biochemistry with Specialization in Bioinformatics

Department of Biochemistry, Microbiology, and Immunology

Faculty of Medicine

University of Ottawa

Abstract

Tumour heterogeneity is a key hurdle for the effective treatment of cancer using oncolytic viruses (OVs). A better understanding of the pathways involved in delineating tumour cell resistance and hypersensitivity to OVs is critical in order to guide the development of new therapeutic strategies to enhance OVs. In this thesis, I performed a comparative genetic and epigenetic study of the murine OV-resistant colon cancer cell line CT26.WT and its hypersensitive subclone CT26.lacZ. This study led to the identification of retroviral insertion sites in AKAP7 and TP53RK genes, that are potentially involved in conveying sensitivity to infection by OVs and the dysregulation of the interferon antiviral response in the CT26.lacZ cell line. Gene overexpression and gene silencing experiments suggest a functional role of these proteins in controlling viral growth. Further investigation of these genes and their relationship to antiviral response pathways is warranted and may lead to novel strategies for improving the therapeutic activity of OVs.

Acknowledgements

I would like to thank my supervisor and mentor Dr. Jean-Simon Diallo for all the help and opportunities that he has provided for me as a student throughout my co-op, honours, and masters projects. I would also like to thank my co-supervisor Dr. Michael McBurney and my thesis advisory committee members, Dr. Marjorie Brand and Dr. Theodore Perkins for the valuable input they provided over the 2 year masters project. I would like to thank Dr. John Bell for originally spiking my interest in oncolytic viruses and bringing me into the lab as an undergraduate co-op student, and Dr. Fabrice LeBoeuf for mentoring me during that time and building my interest in oncolytic virology. Finally, I would like to thank all of members of Dr. Bell's, Dr. Atkins', Dr. Auer's, and Dr. Diallo's labs who have helped out along the way (Rozanne Arulanandam, Nicole Forbes, Rachel McPhedran, Oliver Varette, Andrew Chen, Vanessa Garcia, MOhammed Selman, Dominic Roy, Marie-Claude Bourgeois-Daigneault, Ramya Krishnan, Naveen Haribabu).

Additionally, for this project, I would like to thank our collaborators Dr. Mathieu Lupien and Parisa Mazrooei for providing ChIP-Seq analysis and training me on the techniques used to explore this data.

Table of Contents

List of Abbreviations v
List of Figures and Illustrations vi
List of Tables vii
Introduction 1
1. History of oncolytic viruses 1
2. Mechanism of action of oncolytic viruses 4
   2.1. Oncolysis 4
   2.2. Immune response 5
   2.3. Vascular shutdown 5
   2.4. Transgene expression 6
3. Selectivity of OVs to cancer cells 6
   3.1. Differences between normal and cancer cells exploited by viruses 7
      3.1.1. Metabolism 7
      3.1.2. Defective cell death pathways 7
      3.1.3. Antiviral response 8
4. The type I IFN response 9
   4.1. Pattern Recognition Receptors 9
   4.2. Signalling intermediates 10
   4.3. Interferon Stimulated Genes (ISGs) 11
   4.4. Immunological effects of type I IFN 12
5. Examples of exploiting the Type I IFN response for OV design 12
   5.1. HSV-1 based oncolytic viruses 13
   5.2. Vaccinia Virus 13
   5.3. Semliki Forest Virus A7 14
   5.4. Vesicular Stomatitis Virus Δ51 14
6. Heterogeneity of response to OV therapy 16
   6.1. Pre-clinical evidence 16
   6.2. CT26.WT and CT26.lacZ as a model for heterogeneity of response to OV therapy 18
   6.3. Evidence in clinical trials 18
7. Overcoming resistance to OV therapy 19
   7.1. Viral selection / engineering 19
   7.2. Viral sensitizers 19
      7.2.1. HDAC inhibitors 20
      7.2.2. VSe1 21
8. Sources of heterogeneity in tumour response to therapy 21
   8.1. Genetics 21
   8.2. Epigenetics 22
9. Methods in comparative genomics 24
   9.1. gene expression microarray analysis 24
   9.2. Sequencing 26
      9.2.1. Sanger Sequencing 26
      9.2.2. Next generation chromatin immunoprecipitation sequencing 26
   9.3. Bioinformatic epigenetics tools (SeqPos, ChromHmm) 27
Rational 28
Hypothesis 30
Materials and Methods 30

Cell lines 30
Viruses 31
Statistics 31
Microarray 32
ChIP-Seq 33
Supernatant Transfer 34
Western Blotting 34
Reverse Transcriptase Quantitative PCR 36
Fluorescence Imaging 36
High Throughput Titration 36
siRNA 37
Inverse PCR 37
Results 39
CT26 as a model cell line for studying the characteristics of OV sensitive cells 39
Analysis of the genomic landscape of CT26.WT and CT26.lacZ after infection with OV 42
Analysis of the epigenetic landscape of CT26.WT and CT26.lacZ after infection with OV 48
CT26.WT and CT26.lacZ effectively produce IFNß following infection 52
CT26.lacZ produce functional IFNß but cannot mount an antiviral response 55
JAK-STAT pathway activation in response to infection is defective in CT26.lacZ cells 59
Genetic and Epigenetic determinants of CT26.lacZ sensitivity to oncolytic VSV 65
Isolated CT26.WT subclones exhibit heterogenous sensitivity to infection with VSVΔ51 65
Identification of Genomic integration sites of the LZSN vector in CT26.lacZ 69
Investigation of AKAP7 72
Investigation of TP53RK 76
Discussion 79
Conclusion 90
References 91
Contributions of Collaborators 99
Appendices 100
Curriculum Vitae 101

List of Abbreviations

AKAP	A kinase anchoring protein
ATCC	American Type Culture Collection
bp	Base pair
ChIP-Seq	Chromatin Immunoprecipitation sequencing
DMEM	Dulbecco's Modification of Eagle's Medium
eIF2	Eukaryotic initiation factor-2
ELISA	Enzyme-linked immunosorbent assay
FBS	Fetal bovine serum
Fluc	Firefly luciferase
G	Glycoprotein
GFP	Green fluorescent protein
GM-CSF	Granulocyte macrophage colony-stimulating factor
H3k27ac	Histone 3 Lysine 27 acetylation
H3K4me1	Histone 3 lysine 4 methylation
H3K4me2	Histone 3 lysine 4 dimethylation
H3K4me3	Histone 3 lysine 4 trimethylation
HAT	Histone acetyltransferase
HDAC	histone deacetylase
HPI	Hours post infection
HSV-1	Herpes Simplex Virus 1
IFN	Interferon
IFNAR1	interferon-α/ß receptor 1
IFNAR2	interferon-α/ß receptor 2
IRF3	interferon regulatory factor 3
IRF7	interferon regulatory factor 7
IRF9	interferon regulatory factor 9
ISG	Interferon stimulated gene
ISGF3	Interferon stimulated gene factor 3
L	Large protein
M	Matrix Protein
MAVS	Mitochondrial antiviral signal protein
MHC	Major histocompatibility complex
MM	Mismatch probe
MMLV	Moloney murine leukemia virus
MOI	Multiplicity of infection
N	Nucleoprotein
NGS	Next generation sequencing
NPS	Nucleosome positioning from sequencing
nt	nucleotide
OV	Oncolytic Virus
P	Phosphoprotein
p53 (TP53)	Tumour protein Kinase
PKA	Protein kinase A
PKR	double-stranded-RNA-dependent protein
PM	Perfect match probe
qRT-PCR	Quantitative reverse transcription polymerase chain reaction
RMA	Robust multi-array average
SAHA	suberanilohydroxamic acid
TAA	Tumour associated antigens
TFBS	Transcription factor binding site
TK	Thymidine Kinase
TP53RK	Tumour protein 53 regulating kinase
V600E	BRAF Mutation: Valine at codon 600 for glutamate
VGF	Vaccinia growth factor
VSe	Viral sensitizer
VSV	Vesicular stomatitis virus
VSVΔ51	Vesicular stomatitis virus (matrix protein knockout)
VSVΔ51-ΔG	Vesicular stomatitis virus (Matrix and Glycoprotein knockout)
VV	Vaccinia virus
VVdd	Vaccinia virus double deleted (ΔTK and ΔVGF)
wtVSV	Wild-type vesicular stomatitis virus
X-gal	5-bromo-4-chloro-3-indolyl-β-D-galactopyranoside

List of Figures and Illustrations

Figure 1: *In vitro* infection of CT26.lacZ with Oncolytic VSVΔ51 demonstrates 120 fold higher viral expression compared to CT26.WT ……. 40

Figure 2: Clustered heatmap analysis of the top 1% of genes with greatest fold change post infection with VSVΔ51 ……..…….. 44

Figure 3: Gene-Ontology analysis of unresponsive CT26.lacZ genes ……. 46

Figure 4: ChIP-Seq analysis of transcription enhancer site histone methylation ……. 50

Figure 5: Expression and secretion of IFNß by CT26 subtypes in response to viral infection ……..……..... 53

Figure 6: Supernatant transfer assay measuring CT26 subtypes production of and response to post infection cytokines …...…….…….. 57

Figure 7: Protein quantification of JAK-STAT pathway post infection in CT26 subtypes ……..……..…….. 61

Figure 8: mRNA transcription levels of key JAK-STAT pathway proteins …… 63

Figure 9: Heterogeneous sensitivity to VSVΔ51 infection of isolated CT26.WT subclones ……..…….. 67

Figure 10: LZSN integration sites in the CT26.lacZ genome gel electrophoresis ……... 70

Figure 11: Comparison of AKAP7 variant expression and effect on sensitivity of infection in CT26WT and CT26.lacZ ……..…….. 74

Figure 12: TP53RK transcript expression and siRNA knockdown in CT26.WT and CT26.lacZ ……..……. 77

Figure 13: Illustration of AKAP7 variants and LZSN integration site in CT26.lacZ…... 85

List of Tables

Table 1: Primary antibody details ……..… 35
Table 2: Inverse PCR primers ……..…. 38
Table 3: Identification of genes closest to LZSN integration sites in CT26.lacZ …… 72

Introduction

1. History of oncolytic viruses

Oncolytic viruses are a versatile cancer therapeutic platform owing to the ease of engineering viruses that are tumour selective. Furthermore, they can be used to harness the power of the host immune system for lasting cancer eradication. However, oncolytic viruses were not developed following a single eureka moment. Rather, like many discoveries in biological research, the premise for oncolytic viruses came from coincidental clinical observations in patients that contracted severe infectious diseases while undergoing cancer treatment. These occurrences have been documented since the mid 1800's with numerous scattered reports describing complicating illnesses that coincide with tumour regression and short lived remissions (1). In 1904 Dr. George Dock published a well known study describing 65 cases of cancer patients having improved cancer-associated disease after acute infection. This includes the case of a leukaemia patient who contracted a complicating disease (now believed to be the influenza virus) which led to almost complete cancer remission (1, 2). Considering that the first virus to ever be documented was published in 1892, and influenza was not discovered for another 29 years after Dr. Dock's observations, it is not surprising that it was difficult to fully explain these results with the tools available at that time (3). However, over the years cases continued to be reported, and a later publication in 1958 summed up roughly 350 occurrences of spontaneous remission in leukaemia patients, in which 62 patients remained cancer free for over 5 years (4).

At this point a trend was beginning to emerge as it seemed that mainly patients with late stage leukaemia or lymphomas were developing spontaneous remission/regression events. As these two cancer types are highly immunosuppressive, late stage patients were more likely to pick up a concurrent viral or bacterial infection. Additionally, due to the patient's weakened immune systems, infections could spread more easily within the host, and in some cases lead to clearing of the cancer or tumour mass (5). As the seemingly beneficial effects of concurrent infections in cancer patients were becoming apparent, clinicians tested the use of cortisone immune suppressors in patients in order to increase infection and viral load; a strategy that did show slight improvements in patient cancer related disease status (5). However, these immunosuppressive treatments likely affected many aspects that were beneficial — such as the anticancer immune response — and did not change the fact that patients developing infections were often in a late progressed stage of cancer with little chance of full remission (1, 2, 4, 5).

Around this time, in 1949, an observation of spontaneous remission in three Hodgkin's-lymphoma patients after concurrent hepatitis infections, sparked a group of researchers to test live hepatitis injections in a 22 patient trial. The idea being that if you manually deliver a virus as a therapy before the cancer had progressed, you may obtain a more robust treatment with lasting effects. Unfortunately of the 22 patients treated, only 13 actually developed a hepatitis infection, and only seven of those demonstrated improvements (moderate) in pain or blood cell ratios (6). Despite the poor outcome from that trial, two similar trials were attempted shortly after by different groups, one with 6 patients injected with multiple doses of Epstein-Barr Virus, and a second with 34 patients injected with West Nile virus (7, 8). Once again, few patients developed infection, and those that were infected displayed short-lived initial reduction in tumour mass or

favourable blood cell ratios, followed by a rapid decline in health. From the multiple cases of neurotoxicity, encephalitis, and deaths likely associated with the viral treatment, it became clear that the viruses being used may not be suitable for therapeutic purposes.

Thus, new criteria based around safety and immune activation were prioritized, leading to a new generation of oncolytic virus candidates including adenoviruses, herpes viruses, paramyxoviruses, picornaviruses, and poxviruses (1). In 1955, initial trials with adenovirus demonstrated clear improvements with no cases of encephalitis or virus associated death, lasting infection of tumour tissues, and it was even noted that tissues surrounding the tumours were not getting infected, suggesting a tumour specificity of the virus (9). Similar positive results were seen with the paramyxovirus mumps, which displayed minimal toxicity in all patients and either complete tumour regression or reduction in size to less than half of the tumours initial size (10). However, there were still some issues with these new viruses. Firstly, a significant percentage of the population has already been exposed to these viruses and had developed neutralizing antibodies that will rapidly clear up any viral particles in their body, thereby rendering these viral treatments ineffective against the tumours. Secondly, regulatory boards were wary of the idea of using non-attenuated pathogenic human viruses as a standard of care (1). This sparked the interest for non-human viruses that would solve both issues at once, as they remove the possibility of pre-existing antibodies and reduce the risk of human pathogenicity. This led to the use of bovine Herpesvirus, avian Newcastle disease virus, and bovine Vesicular Stomatitis Virus (VSV); all of which are still being tested as clinical candidates for various types of cancers to this day (11-16).

2. Mechanism of action of oncolytic viruses

Oncolytic viruses lead to a number of physiological effects that contribute to eradicating cancer cells, including oncolysis, stimulation of immune response, and vascular shutdown. Furthermore, some modern oncolytic viruses are engineered to express transgenes that improve one or more of these effects, or provide additional therapeutic or imaging functionalities.

2.1 Oncolysis

The most immediate mechanism of cancer cell eradication by OVs is oncolysis. *Onco-* referring to cancer, and *-lysis* describing the lytic destruction of infected cancer cells. Lysis is natural to the life cycle of many viruses within permissive hosts, allowing for the release and spread of virus particles after replication. In the case of oncolysis, viral infection and replication is targeted to cancer cells through techniques such as virus selection, evolution, or genetic engineering.

Early OV studies focused on maximizing oncolysis of viral therapies by searching for viruses inducing the most cytotoxicity in cancer cells, or by combining treatment with immunosuppressive drugs to improve tumour infection (1, 5) We now understand that there are many other factors including the immune response that are key to OV therapy, however, oncolysis remains a central initiating component of OV therapy. It is generally considered that classical OV treatment cannot be broadly successful if no infection of the tumour is achieved.

2.2 Immune response

Hosts are well adapted to fight off viral infections and possess multiple robust innate and adaptive immune mechanisms to clear pathogens. Oncolytic viruses are able to exploit various cancer hallmarks to replicate selectively within a tumour bed (explained further below) and by doing so, lead to the release of cytokines that attract immune cells in proximity to cancer cells (17). This can effectively overcome the immunosuppressive environment often associated with tumours. For example, reovirus has been shown to activate IFNγ secretion from tumour associated dendritic cells, which in turn induce an antitumour response that promotes cytolytic activity of natural killer cells and T-cell activation (18). The ability to manipulate the host's own immune system against the tumour cells has now become a main focus of modern OVs, with many new virus platforms aiming to maximize the immune stimulatory effect and to direct tumour cell recognition.

2.3 Vascular shutdown

Vascular shutdown is an indirect cytotoxic mechanism of oncolytic viruses that helps induce apoptosis of uninfected tumour tissues. Studies have demonstrated that OVs including VSV and Vaccinia, promote the secretion of pro-inflammatory cytokines that lead to vascular shutdown and reduced blood flow to the interior of a tumour mass (19). While the reduced blood flow slightly inhibits viral spread to the interior of the tumour, vascular shutdown effectively induces apoptosis/necrosis of those malignant cells without the need for direct infection.

2.4 Transgene expression

Transgene expression from oncolytic viruses highlights one of the major strengths of viral therapeutic platforms. The DNA or RNA based nature of viruses and the broad availability of genetic engineering strategies allows for the integration and expression of genes from other organisms or viruses. These transgenes can be used to improve tumour cell targeting, replication, or spread of oncolytic viruses, and typically boost either oncolysis or immune activation. For example, Granulocyte macrophage colony-stimulating factor (GM-CSF) is a host protein normally secreted by immune cells to stimulate local immune activation and is used in several OV platforms. Additionally, Sodium-iodide symporter is an iodine transporter protein that can be used in combination with radioactive iodine treatment for tumour cell targeted radiation therapy as well as a method for non-invasive imaging (20, 21).

However, the most common transgenes incorporated into OV are non-therapeutic markers for tracking or monitoring the virus. For example, green fluorescent protein (GFP), which causes infected cells to fluoresce when excited with light (359 nm wavelength), Firefly luciferase (Fluc) which produces light in the presence of luciferin substrate, or lacZ which changes color in the presence of 5-bromo-4-chloro-3-indolyl-β-D-galactopyranoside (X-gal).

3. Selectivity of OVs to cancer cells

Defects and mutations in cancer cells naturally make them more susceptible than normal cells to viral infection. Oncolytic viruses are selected or engineered to exploit these defects allowing the viruses to be highly attenuated and safe, but still able to infect cancer cells. Explained below are some of the mechanisms that promote viral replication in cancer cells.

3.1 Differences between normal and cancer cells exploited by viruses

3.1.1 Metabolism

Cancer cell metabolism is typically much higher than in normal cells to support constant division and growth. This high rate of metabolism is one of the reasons that current drug therapies are often ineffective in many cancers (22). Alternatively, when using an OV therapy, high metabolism implies elevated availability of nucleotides, gene translation and growth, all of which are beneficial for viral replication. Some OVs, such as Vaccinia Virus (VV) Thymidine Kinase (TK) knockout, have been designed to exploit elevated metabolism of cancer cells as a primary cancer targeting strategy. TK is an enzyme required for making thymidine-phosphate which can be incorporated into DNA. VV virally expressed TK is mandatory for viral replication in normal non-dividing cells where cellular TK expression is low. When VV viral TK is knocked out, it can only be functionally supplemented if the virus has infected an actively dividing cell, such as a cancer cell that expresses compatible host TK (23).

3.1.2 Defective cell death pathways

p53 mutations are present in over 50% of human cancers making them one of the most common cancer associated gene defects (24). In normal cells, p53 is a critical cellular transcription factor that participates in many pathways including, DNA damage repair, apoptosis, and cell cycle arrest. Cancer cells carrying p53 mutations typically harbour persistent phosphorylation of serine 15 that stabilizes dysfunctional p53 and causes it to act in a dominant negative manner (24).

Ultimately, these cells lose the ability to trigger cell cycle arrest and apoptosis, thereby beginning the process of uncontrolled cell proliferation and oncogenesis.

Interestingly, to improve viral pathogenicity, many viruses encode genes that directly or indirectly inhibit p53 in a similar fashion to the p53 inhibition observed in cancer cells (25). This provides a growth advantage for many viruses in cancer cells with p53 mutations as these cells will not trigger apoptosis and provide a better chance for the viruses to complete their life cycle.

3.1.3 Antiviral response

Antiviral defence pathways are antithetical to the immune evading and hyper-proliferative phenotype of cancer cells. For example, IFNs secreted during antiviral response stimulation are both antiproliferative and immunostimulatory (26).

Due to these anticancer properties, IFNs have previously been tested and administered as a therapeutic, in an attempt to block proliferation and promote apoptosis of tumour cells. However, most cancers have been found to harbor defects in IFN signalling pathways, likely to abrogate any of the above mentioned impediments to cancer progression (26, 27).

Another antiviral pathway commonly affected in cancer cells involves double-stranded-RNA-dependent protein (PKR). PKR is a protein activated under cellular stress that inhibits eukaryotic initiation factor-2 (eIF2) and induces inhibition of cellular translation (28). This mechanism is normally used as an antiviral response that blocks translation of viral genomes, but can act as a potent barrier to the progression of many cellular stresses including oncogenesis. Therefore, cancer cells often contain mutations in Ras family proteins, which lead to inhibition of PKR and abrogate its antitumour, and also antiviral potential (26).

Many viruses encode genes that inhibit proteins such as PKR and components of IFN response to allow for infection, replication, and spread within a host. However, by exploiting these mutations found within the cancer cells and knocking out the inhibitors expressed by the viruses, we can create selective viruses that are only able to infect cancer cells and not the host's normal cells.

4. The type I IFN response

The type I interferon response pathway is a primordial innate cellular defence mechanism against viral, bacterial, and fungal infections, and is present in all cell types (29, 30). It is a highly sensitive pathway able to detect small amounts of foreign material and quickly warn all nearby cells to mount defences by activating the transcription of hundreds of interferon stimulated genes (ISGs) before those cells become infected (30). There are seven classes of type I interferons (eight in mice) IFNα , IFNß, IFNε, IFNτ, IFNκ, IFNω, IFNδ and the mouse only IFNζ (31). Depending on the stimulus, a cell can secrete different classes of IFN cytokines to signal for different downstream events. In the case of a viral stimulus the main IFN classes secreted are IFNα and IFNß, however, due the redundancies in these two cytokines and the dominant role of IFNß, in this thesis I have focused on IFNß as the type I interferon of interest (32).

4.1 Pattern Recognition Receptors

Pattern Recognition Receptors are the initiators of the type I IFN response, and are composed of a functional group of receptor proteins that sense foreign material, such as viral

genomes or proteins, in and around the cell. Membrane-spanning toll-like receptors identify viral protein patterns through pathogen-associated molecular patterns; cytosolic DNA is sensed through proteins such as cGAS , IFI16 , DAI proteins; and double stranded RNA is detected by the RIG-I-like receptors, RIG-I and MDA5 (30, 33). In the case of an RNA virus infection, RIG-I/MDA5 will sense double stranded RNA during viral replication and activate the RIG-I/MDA5 complex. The activated complex then binds to mitochondrial bound mitochondrial antiviral signal protein (MAVS) which undergoes a prion-like change in conformation that propagates to activate other nearby MAVS proteins, thus resulting in an amplification of the RNA sensing signal (30, 34). The amplified MAVS signal leads to activation of kinases TBK1-IKKε, followed by phosphorylation of interferon regulatory factor 3 (IRF3) and interferon regulatory factor 7 (IRF7) causing them to translocate to the nucleus and activate the transcription and secretion of IFNα and IFNß (30, 31).

4.2 Signalling intermediates

The second phase of the type I IFN response involves passing on the viral infection warning signal to other nearby cells via the IFN cytokines. The receptor complex for type I IFN is made up of several components including interferon-α/ß receptor 1 and 2 (IFNAR1 and IFNAR2), and kinases Jak1 and Tyk2, which covalently associate to IFNAR2 and IFNAR1 respectively, on the cytosolic side of the membrane. Specifically, IFNß first binds to IFNAR2 which has stronger affinity for type I interferons. This then promotes the dimerization with IFNAR1 and triggers Tyk2 mediated phosphorylation of IFNAR1 on its cytoplasmic tail at tyrosine 466 (35, 36). Following this, STAT2 binds to the cytoplasmic tail of IFNAR1 via its

SH2 domain, and is phosphorylated by Tyk2 on tyrosine 690. Activated STAT2 then acts as a scaffolding for STAT1 recruitment, which upon Jak1 mediated phosphorylation of tyrosine 701 arranges into an antiparallel heterodimer with STAT2, each with their activated phosphotyrosine residues binding to the SH2 domain of one-another (35, 37, 38).

The STAT1/STAT2 heterodimer then recruits the interferon response factor 9 (IRF9), to form the interferon stimulated gene factor 3 (ISGF3) complex which traverses nuclear pores where it functions as a transcriptional activator of hundreds of antiviral interferon stimulated genes (ISGs). The core complex of ISGF3 is composed of STAT1/STAT2/IRF9, however, several other components are often incorporated such as histone deacetylases, histone modifying enzymes including p300 and Creb Binding Protein (39, 40), while STAT2 is known to integrate histone acetyltransferases PCAF and GCN5 (41).

After the upregulation of type I IFN response and the formation of ISGF3, a series of negative feedback pathways signal the recycling of IFNAR1/2 receptors, nuclear export of STAT1/2, and dephosphorylation of activated proteins, to halt the ongoing antiviral response (37, 42).

4.3 Interferon Stimulated Genes (ISGs)

ISGF3 binds to interferon stimulatory response element (ISRE) that promotes the transcription of several hundred interferon stimulated genes (ISGs). This plethora of ISGs will rapidly affect cellular processes to stop cell proliferation, halt translation, and trigger apoptosis. For example, PKR discussed previously is an ISG able to inhibit all cellular translation by phosphorylating eIF2α in the presence of double stranded or viral uncapped RNA (43).

Additionally, many of the upregulated ISGs specifically target the infecting viruses and their genomes. MX1 and MX2 ISGs trap virions inside ring-like structures to sequester them from their cellular destinations (44). 2'-5'-oligoadenylate synthetases activate RNase L to initiate degradation of cytoplasmic RNA including viral genomes (45). IFN-stimulated gene 20 kDa is an exonuclease that directly degrades viral genomes such as VSV, influenza, and encephalomyocarditis (45, 46). Finally, APOBEC3 and ADAR1 rapidly mutate any double stranded RNAs present in the cell by editing all cytidines to uridine and adenosines to inosine respectively (45, 46). This outlines some of the most studied ISGs, however, many other ISGs still have unknown functions and contribute to the cellular antiviral state.

4.4 Immunological effects of type I IFN

In addition to the activation of ISG's through JAK-STAT signalling, studies have also shown that IFNß leads to the activation of myeloid cells, T cells, B cells, and natural killer cells. This allows IFNß to simultaneously alert nearby cells of viral infection in order to mount innate antiviral defences that slow and impede viral spread, while also activating the innate and adaptive immune system to clear the virus and develop a lasting resistance to infection (47).

5. Examples of exploiting the Type I IFN response for OV design

Modern OVs are selected or engineered to optimize their safety and oncolytic potential. As discussed in section 3 OVs typically accomplish this goal by exploiting differences in cancer cell metabolism, cell death regulation, and defective antiviral responses. Here we expand on some noteworthy and current clinical OV candidates.

5.1 HSV-1 based oncolytic viruses

Herpes Simplex Virus 1 (HSV-1) based OV platforms have emerged as strong contenders for clinical viability, especially in the treatment of melanoma. T-Vec, the forerunner candidate has recently completed phase 3 trials for efficacy and safety in a 436 patients (Clinical Trial: NCT00769704), and has early support to gain FDA approval in the near future. T-Vec is based on HSV-1 virus serotype JS-1 and has been engineered to express GM-CSF to boost its immune activating potential by recruiting dendritic cells to the tumour site (48). Additionally, the genes ICP34.5, which inhibits PKR activation, and ICP47, which blocks antigen presentation on major histocompatibility complex class I and II (MHC-I and MHC-II), in wild-type HSV-1 have been knocked out in T-Vec to boost oncolytic and immunogenic properties (49). Finally, T-Vec also has a modified US11 gene that is expressed earlier in the viral life cycle than in wild-type HSV-1, resulting in a boost to viral replication (49, 50).

5.2 Vaccinia Virus

Vaccinia virus is a large DNA virus that can be easily engineered to express transgenes and/or manipulated to knockout viral genes. In the process of working with Vaccinia virus, many interesting antiviral genes within its large viral genome have been identified. For example, the B18R protein functions to aggregate and remove type I IFN cytokines secreted from infected cells and ultimately blocks type I IFN signalling (51). This gives Vaccinia a spreading advantage as the nearby cells cannot prime antiviral defences in preparation for infection. Purified B18R has even been used in combination with other OVs such as VSV and results in highly synergistic

increases in viral titers and in vivo efficacy of the oncolytic treatment while maintaining tumour cell selectivity (52).

Pexa-Vec, is a VV clinical candidate based on the Wyeth VV strain. This strain naturally harbors a mutation in B18R gene and does not inhibit type I IFN signalling, therefore in this case generating a more safe therapeutic (53). Additionally, Pexa-Vec has been attenuated with a TK deletion (23). As described previously, TK is required for viral replication, meaning that knocking out the gene causes the virus to rely on its cellular host to provide TK.

5.3 Semliki Forest Virus A7

Semliki Forest Virus strain A7 (SFV-A7) is an enveloped positive stranded RNA virus that is not genetically engineered and was selected for its natural oncolytic potential. Some strains of SFV do infect humans, however while SFV-A7 has no impact on mature adult cells, it is capable of selectively infecting cancer cells. Additionally, SFV-A7 oncolytic efficiency is independent of p53 status, a factor which normally affects the replication cycles of many other OVs (54).

5.4 Vesicular Stomatitis Virus Δ51

Vesicular stomatitis virus (VSV) is a single-stranded negative sense RNA virus belonging to the rhabdoviridae family (55). VSV is an insect virus, however while its primary reservoir is in sandflies, the virus (VSV) has a broad host range which includes many mammalian species such as horses, cattle, and swine (55). VSV infection in humans is non-fatal and and leads to influenza-like symptoms (55). The VSV genome is 11 kb long, and encodes for 5 proteins,

nucleoprotein (N), phosphoprotein (P), matrix protein (M), glycoprotein (G), and large protein (L), arranged in that order 5' to 3' (56). In the junction between each gene sequence resides a short polyadenylation signal and a conserved dinucleotide stop signal that temporarily interrupts progression of the viral polymerase resulting in a gradient of protein expression along the genome with the first protein, N as the most abundantly produced viral gene, and L as the least abundant (56, 57). VSV virions bind to low-density lipoprotein receptor and its family members that are highly abundant on the surface of many cell types (58). This causes the internalization of the virions through endocytosis over a period of 1-2 minutes (58-61). During endocytosis the pH inside the endosome drops, thereby catalysing a reaction (pH < 6.17) that causes VSV glycoproteins to polarize at either end of the virion and expose a central hydrophobic domain which then binds to the endosomal membrane (55, 62, 63). The viral RNA coated in N, L, and P proteins enter the cellular cytoplasmic space, whereas M protein moves into the cell cytoplasm (55, 61). The major function of the M protein is to block the transport of proteins, mRNA, and rRNA across the nuclear membrane. This mechanism allows VSV to stop all cellular translation, and effectively inhibit the host's antiviral response (64). In an effort to maximize the oncolytic potential of VSV and simultaneously attenuate its pathogenic properties, site directed mutagenesis of the VSV Indiana strain was used to delete methionine codon at position 51 in the viral M protein amino acid sequence to generate the oncolytic virus VSVΔ51. The Δ51 mutation abrogates the capacity of viral M protein to inhibit nuclear export of cellular antiviral mRNAs including IFNs. Due to VSVs high sensitivity to IFN, this mutation severely attenuates VSVΔ51 in normal human cells, however, the virus retains its ability to infect most cancer cells as they often already harbor cancer related defects in interferon production or signalling (65). In

summary, VSVΔ51 is a cancer specific virus that is engineered to leave normal tissues unscathed while effectively spreading in cancer cells as a safe targeted oncolytic viral therapeutic.

6. Heterogeneity of response to OV therapy

6.1 Pre-clinical evidence

OVs are selected or designed to be both safe and effective in a broad range of cancer cell lines. However, due to the vast amount of heterogeneity in cancers and the many various paths leading to oncogenesis, OV therapies are not always effective in every cancer type. For example, the NCI60 is a panel of 60 human cancer cell lines commonly used to assess the range of cancer therapeutics across multiple cancer types and variants. VSVΔ51 has been reported as effective in 83% (47 of 57) NCI60 cell lines, VSV-IFNß is only effective in 33%, and Vaccinia Virus has general broad range of efficacy across the panel, but fares worse in leukemias (65-68).

Even in cancer subtypes normally treatable by a particular OV, some cancer cells within a population maintain residual antiviral activity rendering them resistant to the therapy (27). Intra-population heterogeneity of cell lines is well known even in normal cells by the viral manufacturing field, where cell lines are often subcloned to obtain the most sensitive variants from within the population for production (69).

6.2 CT26.WT and CT26.lacZ as a model for heterogeneity of response to OV therapy

Recently, Ruotsalainen et. al. reported a study comparing the viral sensitivity of the mouse colon cancer cell line CT26 (herein referred to as CT26.WT) to its subcloned cell line CT26.lacZ (also known as CT26-CL25) (70). CT26.WT and CT26.lacZ, are commonly used

mouse tumour model cell lines that originate from a 1995 study by Wang et. al. who observed that many tumour cells expressed antigens that were not recognized by T lymphocytes. They hypothesized that through a vaccination approach, they could train the host's immune system to recognize these tumour associated antigens (TAA) and direct the host's own immune system towards clearing the tumour burden in a selective fashion. To asses their cancer vaccine hypothesis, Wang et al. created the CT26.lacZ model cell line engineered by retroviral transduction to express ß-galactosidase as a synthetic TAA. ß-galactosidase was chosen as the TAA as it was well characterized and used in multiple antigen related studies previously, such as antigen localization and processing (71). Additionally, ß-galactosidase is commonly used as a tumour cell metastasis marker and has been shown to have little to no effect on the tumour growth or lethality (71).

CT26.WT, an N-nitroso-N-methylurethane-induced colon carcinoma syngeneic to BALB/c, was chosen as the model platform due to its high cancer-specific lethality when injected in mice through various routes. To stably express lacZ, the authors used the LZSN retroviral vector derived from Moloney murine leukemia virus (MMLV) to transduce the CT26.WT cells (71,72). The LXSN vector contained the lacZ gene under transcriptional control of a 5' long-terminal repeat followed by a SV40 promoter-driven neomycin resistance gene (71). Transductants were screened for neomycin resistance using media containing G418, followed by single cell clonal selection by limiting dilution. CT26.CL25 (referred to as CT26.lacZ in this thesis) was selected as the clone with the highest production of ß-galactosidase. The authors further demonstrated that both CT26.WT and CT26.lacZ had similar growth rates and were equally lethal in mouse models (71).

Stable expression of ß-galactosidase in CT26.lacZ allows for easy visualization of metastases, and has made CT26.lacZ a very popular cell line used in over 160 studies published to date. CT26.lacZ are often assumed to be equivalent to CT26.WT, however, other than the general phenotypic observations of growth and lethality originally reported by Wang et. al., no further comparative analyses have been performed until recently. A 2015 study by Ruotsalainen et. al. identified radical differences in the amount of infection observed in CT26.WT and CT26.lacZ when using oncolytic Semliki Forest virus VA7 (70). The authors confirmed that CT26.WT cells were able to mount a standard type I IFN response that drives the strong resistance of CT26.WT to VA7 infection. In contrast, CT26.lacZ failed to phosphorylate STAT1 (a central type I IFN signalling component), which leads to failure to induce ISG expression and explains CT26.lacZ cell lines high sensitivity to VA7 infection and spread (70). Most importantly, this drastically changed the therapeutic outcome of VA7 treatment as demonstrated in both immunocompetent and severe combined immunodeficient mice, where a single dose of VA7 cures mice harbouring CT26.lacZ tumours, but never cures mice with CT26.WT tumours (70).

6.3 Evidence in clinical trials

These same heterogeneous responses to OV treatment are also prevalent, if not more so, in clinical trial data. T-Vec while highly successful in some patients, only demonstrated response (partial and complete) in 37% of treated patients (73). Another clinical OV candidate Pexa-Vec based on the VV platform, resulted in 62% response rate in patients (74). In both studies the

virus was administered intratumorally, suggesting the variability in response is unlikely attributable to heterogenous delivery.

Interestingly, there is always a subset of patients that do not respond at all to OV therapy while other patients are being cured with the same dose of virus. It is of course possible that some of the patient's disease was too clinically advanced or had suppressed immune systems from previous chemotherapeutic treatments, however the results still suggest that there is a broad heterogeneity in the response of patients to OV therapy.

7. Overcoming resistance to OV therapy

7.1 Viral selection / engineering

Further genetic engineering can be applied to incorporate additional or different transgenes in an effort to boost oncolysis or immune activation. However, this can be difficult with small RNA genome viruses as they can often only incorporate one or two transgenes at most. An alternative technique is to search within the phylogenetic family of a current oncolytic virus to identify other serotypes that may have improved cytotoxic capacity in cancer cells while maintaining tumour cell selectivity. This process was performed to select VA7 strain for SFV for use as an oncolytic virus, as well as to discover Maraba MG-1, a novel alternative to VSVΔ51 currently being tested in phase I clinical trials (75) (Clinical Trial: NCT02285816).

7.2 Viral sensitizers

Another technique for overcoming tumour cell resistance to OV therapy is combination with small molecule viral sensitizers (VSe). VSes can functionally mimic virulence genes and

temporarily “sensitize” tumour cells for subsequent oncolytic virus treatment. Additionally, because VSes are administered independent of the oncolytic virus, they can be dose controlled and administered for various time periods depending on the needs of the individual patients. This greatly improves therapeutic safety and provides a broader range of application without the need for numerous variations of viruses.

VSes have been shown to raise viral titers *in vitro* as much as 1000 fold in tumour cells, and enhance the efficacy of IFN-sensitive oncolytic virus VSVΔ51 in human tumour explants while remaining safe to normal tissues (27).

7.2.1 HDAC inhibitors

Histone acetylation is an epigenetic activation marker that signals open chromatin formation and allows access to the underlying genetic code for transcription factors and replication machinery. Therefore, histone acetyltransferases (HAT) normally cause increased gene expression, whereas histone deacetylases (HDAC) close down chromatin structure and lead to transcriptional repression (76). Interestingly, small molecule HDAC inhibitors were some of the first “viral sensitizers” characterized and function by inhibiting IFN-induced up-regulation of ISGs resulting in improved viral infection. For example, CT26.WT treated with the HDAC inhibitor suberanilohydroxamic acid (SAHA) become as sensitive to viral infection as CT26.lacZ. Additionally, no significant increase in viral titer is observed in CT26.lacZ cells that are treated with SAHA (unpublished data). Interestingly, the JAK-STAT pathway transcription factor ISGF3 requires HDACs to act as a transcriptional activator and to properly recruit RNA polymerase II to gene transcription start sites (76, 77).

7.2.2 VSe1

Viral Sensitizer 1 (VSe1) identified by Diallo et. al. in 2010 following a high-throughput drug discovery screen is one of the flagship VSes studied in our lab for synergy with OVs. Pretreatment with VSe1 inhibits ~96% of the cellular antiviral transcripts induced by VSVΔ51 infection, but does not inhibit IFNß secretion (27). Therefore, rather than substituting the viral M protein of VSVΔ51, VSe1 inhibits the spread of antiviral signals to nearby cells, likely by targeting the JAK-STAT signalling cascade. VSe1 also sensitizes CT26.WT cells to viral infection with VSVΔ51, rendering them as sensitive as untreated CT26.lacZ cells. Similar to SAHA, VSE1 has no additional sensitization effect on CT26.lacZ cells.

8. Sources of heterogeneity in tumour response to therapy

8.1 Genetics

Genetic heterogeneity is elevated in cancer cells due to their common dysfunction in DNA repair and DNA replication pathways (78). This genetic heterogeneity within tumour populations poses a serious hurdle for many cancer therapeutics, as they may induce pressured selection of drug-resistant subpopulations.

For example, mutations in the BRAF gene account for 30% of human cancers and 40% of melanomas (79). The most common of these mutations is the replacement of valine 600 to glutamate (V600E). The small molecule drug vemurafenib was designed to inhibit only BRAF V600E mutants and not affect normal BRAF, resulting in a cancer cell selective inhibition of BRAFs downstream target ERK, which leads to cell death (80). However, due to genetic

heterogeneity, a subset of cells express a 61 kDa version of BRAF that is resistant to vemurafenib and maintains ERK activation, therefore evading cell death (80).

While oncolytic viruses have much broader targeting mechanisms than small molecules, it is still possible that genetic heterogeneity could lead to OV resistance. Comparative genetic analysis of cancers that are resistant to those that are sensitive to a therapeutic can help define biomarkers to direct personalized medicine and also to drive the development of novel therapies that avoid the development of resistance.

8.2 Epigenetics

In addition to genetics as mentioned above, epigenetics also contributes significantly to heterogeneity in a population of cells. Epigenetics is the study of non-permanent phenotypic modifications through factors such as histones that associate with DNA to direct structure and interaction with other proteins. Unlike the permanent changes to gene expression incurred by mutations in genomic DNA, epigenetic changes allow cells to modify gene expression in a temporary fashion. It is now well understood that epigenetics has a central role in gene expression, is key to regulating differentiation of cells, and leads to heterogeneity in cell populations (81). Epigenetics regulate cell processes in many ways, such as through modifications of nucleotides (methylation) to recruit or block proteins that bind to DNA, histone modifications (methylation, acetylation) that disrupt or change chromatin structure, and changes to nucleosome components to influence DNA packaging (81-83).

Recent technological advances have fueled rapid progress of epigenetic studies, mainly due to the advent of chromatin immunoprecipitation sequencing (ChIP-Seq), which allows for

fast and accurate mapping of epigenetic marks across the entire genome. ChIP-Seq is performed by cross linking DNA-bound proteins in place, followed by shearing or digesting the unbound DNA, precipitating out proteins of interest with a specific antibody (for example a histone with a specific methylation mark), and finally purification the DNA bound to the protein of interest for sequencing by next generation sequencing (NGS).

The histone code supports that modifications to histone tails coordinate chromatin structure and can inhibit or recruit proteins to specific locations in the genome, ultimately regulating gene transcription. For example, Histone 3 Lysine 4 monomethylation (H3K4me1) is a marker of genomic enhancer sites and overlaps with p-300 enhancer regions (82). Histone 3 Lysine 4 dimethylation (H3K4me2) is a marker of transcription factor binding sites which results in open chromatin formation allowing transcription factors to bind. On average, 90% of known transcription factor binding sites overlap with H3K4me2 (82). Histone 3 Lysine 4 trimethylation (H3K4me3) is a marker of active promoters and overlaps with RNA polymerase II sites (82). Histone 3 lysine 27 acetylation (H3K27ac) signals active gene promoters and is countered by DNA methylation, a gene silencing mark, which causes the removal of H3K27ac (84).

A 2012 study shows the relationship between genetic mutations and epigenetic states, and highlights the influence of H3K4me1 and H3K4me2 epigenomes in development of breast cancer (85). By analysing one or many of these epigenetic marks in a cell line, we can gain important information that cannot be determined through standard genetic analysis. Additionally, epigenetic analysis is critical to any scientific study observing heterogenous populations, due to the plasticity of epigenetic marks and the strong role that they play in the development of population heterogeneity.

9. Methods in comparative genomics

9.1 Gene expression microarray analysis

Microarrays are well established for measuring gene expression data, however, the preprocessing and data analysis are critical for obtaining quality results. Many options are available and will differ depending on the type of array-chip used, however, robust multi-array average (RMA) is a widely accepted standard practice for preprocessing data before comparative analysis when using affymetrix genechips. This method will help minimize the many factors that can affect data obtained from a microarray experiment, including differing quantities of RNA per sample, differences in fluorescent dyes used to label probes, variations in detection efficiency depending on order or reading or machines used (86).

There are three steps involved in preprocessing, background correction, normalization, and summarization. Background correction in the RMA algorithm is a subtractive process. The observed signal (*s*) is actually a sum of both the true probe intensity (*i*) and a background intensity (*b*). Therefore to obtain *i*, we subtract the background value *b*, which we can estimate taking the mean of mismatched (MM) control probes, from the observed value *s*. However, some adjustments are made to avoid the possibility of a negative true probe intensity *i* (which would happen when the observed value *s* was lower than the mean of the background *b*), which would be unable to convert to log2 scale for the next steps in preprocessing. This is done by assuming that *i* is exponential and *b* is linear, and calculating *b* of each probe in relation to each *s,* as well as imposing that *s* can never be equal to or less than 0 (87). This is noted in the original paper as not being a optimal solution but they defend that it does not introduce any significant or even noticeable error into the data.

The second step of preprocessing is normalization. This ensures that the probe intensities across all samples are measured equally to reduce and biases such as varied binding efficiencies to the probes, differences between chips, or variances in sample preparation and loading. The standard normalization technique used with RMA is quantile normalization. The goal of quantile normalization make the distribution of probe intensities consistent across all chips in an experiment. This is performed by placing the data into a large table with each sample as a column and each probe as a row. Each of the columns are sorted individually (keeping track of their original order) from highest to lowest. Following the sorting, each row is replaced with the mean value of that row. Finally, the sort order is reversed again however the distributions of every chips probe value will be identical (88).

The third and final step is summarization. This step combines measurements from multiple probes into a probeset using Tukey's median polish, a robust averaging method that reduces outliers and further normalizes the across array data by separating the probe effects μ from array effects α. Summarization is performed on log2 transformed probe intensities and thus μ represent the log2 expression value of a probeset (87). After preprocessing, data is annotated by mapping each probeset to its target gene.

Due to the vast amount of data obtained from a microarray experiment and the many factors contributing to a single gene being up or downregulated, it is more efficacious to observe patterns in groups of data instead of single targets. For example, in the case of a gene knockout mutation, we expect that the rest of the pathway, especially downstream genes will also demonstrate dysregulation and be easily identifiable. Enrichment analysis entails filtering out a subset of the data, usually a strict cut-off at 2-fold dysregulation, or by a statistical method such

as standard-deviation or variance. From the enriched data, clustering analysis allows for the identification of patterns within the gene signatures between samples. This can help focus on a specific response pattern of interest and remove noise from the enrichment data. Finally, gene-ontology allows for the classification of a subset of genes into cellular processes to identify dysregulated pathways for further analysis.

9.2 Sequencing

9.2.1 Sanger Sequencing

Sequencing of small genomic regions of roughly one hundred to a thousand nucleotides can be performed by Sanger sequencing method. Each a forward and reverse reaction are performed with primers identical to those used in PCR applications. Elongation is performed by a DNA polymerase with a nucleotide mixture containing terminating dideoxynucleotides with color coded fluorescent fluorophores identifying each nucleotide type . The reaction can then be run through an size separating electrophoretic gel to identify the sequence, either manually, or more commonly nowadays by a computerized sensor.

9.2.2 Next generation chromatin immunoprecipitation sequencing

NGS technologies can sequence millions of segments in parallel and cover entire genomes. ChIP-Seq uses NGS to map the locations of the genome where each of the histone marks were located. For example Illumina sequencing uses short 200-500 bp segments of the DNA and binds them to the surface of chip. Using bridge amplification, each segment PCR amplifies itself multiple times and binds each amplicon into a DNA colony around the original

segment (89). Through controlled addition of a single fluorophore tagged nucleotide per cycle, the system can identify the sequence of millions of DNA colonies at a time. Model-based Analysis for ChIP-Seq (MACS program (90)) was used for peak calling of marked histone locations in the ChIP-Seq data.

9.3 Bioinformatic epigenetics tools (SeqPos, ChromHmm)

Many bioinformatic tools have been developed to analyze various types of ChIP-Seq data. ChromHmm is a powerful program which uses a hidden Markov model to generate output states based on only the data obtained from ChIP-Seq and no other input (unsupervised). This system is designed to take various different epigenetic marks from a single sample source; however, as the authors note, it is also applicable as a comparative epigenetics tool for contrasting multiple samples or cell types against each other.

In this approach, the genome is cut into 200 base pair non-overlapping segments, which represent roughly the occupation of a single nucleosome. Each segment is individually assessed for either presence or absence of a histone mark (91, 92). A set number of states are defined for the model, which generates a probability distribution for the combination of marks in each state. The 200 bp segments are then sorted to a state based on the presence or absence of marks and the probability distribution for each state, as well as the probability of switching from the previous segments state (current state) to the new state (91, 92).

As described above, H3K4me2 ChIP-Seq is enriched at genomic locations containing transcription factor binding sites. SeqPos, another bioinformatic program was designed to search through H3K4 peak data and discover enriched transcription factor binding motifs within peak

regions. Nucleosome positioning from sequencing (NPS) algorithm is used to determine the center of a nucleosome-bound position. Because a nucleosome wraps 146 nt around itself, the NPS algorithm offsets by half of that length (75 nt) from the histone mark 5' end to estimate the center of a bound nucleosome (93). From this center point, a 400 bp nucleosome region is defined as 200bp up and downstream of the centre (94). When a pair of nucleosomes regions overlap each other, the overlapping region is searched by SeqPos for transcription factor binding motifs (95).

Rationale

A major hurdle in the oncolytic virus field is that some patient tumours are resistant to viral infection and may not respond to a given OV treatment. Owing to their mechanisms of action, we expect that oncolytic virotherapy will be maximally effective in virus sensitive tumours. However, currently it is difficult/impossible to identify if a patient's tumour will be sensitive or resistant to viral therapy *in vivo*. Hence we end up with unpredictable and highly variable therapeutic outcomes from patient to patient, highlighting the need to understand the causal factors that underpin sensitivity/resistance. To this end, comparative studies in tumour models that are highly similar but lead to drastically different therapeutic outcomes can be very informative.

Based on their similarity, we wished to determine whether CT26.WT and CT26.lacZ would reproduce the viral resistance and sensitivity phenotypes described by Ruotsalainen et al. when infected with the oncolytic virus candidate VSVΔ51. Furthermore, we were interested in

exploiting the genetic similarity of CT26.WT and CT26.lacZ, to conduct a comparative analysis detailing the mechanisms at the root of CT26.lacZ viral sensitivity, and direct the development of novel OV strategies and potential VSe targets.

Ruotsalainen et. al. showed that CT26.WT and CT26.lacZ exhibit marked differences in their sensitivity to VA7 and identified STAT1 as a likely contributor to this phenotype/outcome. However, given that VA7 is not being pursued clinically, we considered it more relevant to determine whether this observation could extend to more clinically advanced viruses such as VSV and related rhabdoviruses. This seemed likely given that both VSV and VA7 are small single stranded RNA viruses that are highly sensitive to IFN. If the CT26 sensitivity/resistant model were to be confirmed, this could provide an opportunity for uncovering causal factors responsible for differential sensitivity to oncolytic rhabdoviruses and potentially STAT1 dysregulation. The fact that CT26.lacZ is a subclone of CT26.WT, and the observation that HDAC inhibitors can increase the infection of CT26.WT but not CT26.lacZ, suggested a potential implication of epigenetic factors in this phenomenon. Consequently, we considered that a top down genetic and epigenetic analysis of factors that display differing profiles between the CT26.WT and CT26.lacZ should be performed in parallel.

Overall, we considered that understanding the mechanism of viral resistance and sensitivity in cells could provide new directions for the development of future oncolytic viruses and viral sensitizers. Potentially, the identification of new factors involved in the resistance to viral infection could also aid in the development of new antiviral therapies.

Hypothesis

Sensitivity to viral infection observed in the CT26.lacZ cell line, and not their parental CT26.WT cell line, is caused by epigenetic variations that affect the expression of antiviral response genes, selected for during single cell isolation of CT26.lacZ.

Materials and Methods

Cell Lines

CT26.WT (ATCC: CRL-2638), CT26.lacZ (ATCC: CRL-2639), 293T (ATCC: CRL-3216), and vero (ATCC: CCL-81) cells were obtained from the American Type Culture Collection (ATCC) and passaged in Dulbecco's Modification of Eagle's Medium (DMEM) (Corning Cellgro: 10-013) that was supplemented to a final concentration of 5% fetal bovine serum (FBS). T-REx-293 cells (Thermo Fisher) express viral G protein under a tetracycline inducible promoter, which can be activated by pretreating with tetracycline 12 hours before infection. T-REx-293 cells were grown in DMEM containing FBS in addition to zeocin and blasticidin. Subclones of CT26.WT were isolated by limiting dilution at 0.8 cells per well with DMEM 5% FBS mixed 1:1 with supernatant of CT26 cells filtered through 0.45 μm to remove any contaminating cells. Wells containing single cells were identified by brightfield microscopy and were grown until confluency in a 15 cm tissue culture plate.

Viruses

Indiana serotype VSV (wtVSV, VSVΔ51, VSVΔ51-ΔG) viruses were used through this study. VSVΔ51 contains a mutation in methionine 51 of the viral M protein to abrogate M protein inhibition of translation in host infected cells. VSVΔ51-ΔG contains a mutation in viral G proteins and is replication-competent, but cannot not exit the cell or produce infectious virions. GFP and Fluc transgene expressing viruses are recombinants of the VSV viruses listed above (65). For virus amplification, wtVSV and VSVΔ51 were propagated in vero cells for 20 hours, supernatants collected and passed through 0.22 μm vacuum filter to remove cell debris and purified in a 5%-50% optiprep gradient. VSVΔ51-ΔG was amplified in T-REx-293 cells. VSVΔ51-ΔG infected cell supernatants were collected and passed through 0.22 μm vacuum filter to remove cell debris and centrifuged at 30,100 xg to pellet virus. Pelleted virus was resuspended in 1 ml of PBS .

Statistics

Statistical details are explicitly listed for each individual study. Calculations were performed in R, Prism, GOrilla, ChromHMM, and SeqPos. For all studies 95% confidence was required for significance ($p < 0.05$), adjusted p-values accounting for multiple comparisons were used when applicable.

Microarray

Microarray analysis was performed on both CT26.lacZ and CT26.WT to study their transcriptional response post viral infection. Both CT26 cell lines were infected with VSVΔ51 virus at an MOI of 0.01 as well as mock infected with media (control) in 15 cm tissue culture dishes. Samples were collected 24 hours post infection and processed on Affymetrix Mouse gene 1.0 ST arrays. Data analysis was performed in R using the oligo package (96). Data was normalized using the robust multi-array average for background correction, utilizing a quantile normalization, and median-polish summarization to reduce noise due to array effects. Probe intensities were evaluated using the "core" method to estimate log2 expression values of genes at the transcript level. Fold change was then calculated by subtracting the Mock sample from the VSVΔ51 infected sample for each cell line. The top 1% most dysregulated genes were selected from the dataset by calculating CT26.WT fold change post infection minus the absolute value of CT26.lacZ fold change (this equated to genes with a differential expression of larger than 3.26). Other comparisons such as uninfected CT26.WT vs. uninfected CT26.lacZ were also performed but did not yield any significant results. The 1% filtered dataset was then clustered into groups of genomic expression profiles using Euclidean distance with complete linkage, plotted as a heat map in Figure 2. To expand the red cluster of interest (CT26.lacZ genes that are minimally changed when CT26.WT genes are highly induced) we filtered a new set of genes from the dataset using the criteria:

$$CT26.WT - |CT26.lacZ| \geq 1$$

where CT26.WT and CT26.lacZ are the log2 fold change values of each gene. This resulted in a list of 73 genes that were then sorted by CT26.WT log2 expression and plotted on a heat map (Figure 2). Gene Ontology analysis was performed by two unranked lists with the 73 genes as the target and the full microarray gene list as a background set in the online tool GOrilla (97, 98). Results from GOrilla were reduced through similarity using Revigo (99). Significant terms are visualized by -log10(p-value) in Figure 3.

ChIP-Seq

Chromatin Immunoprecipitation (ChIP) was performed on uninfected CT26 cells as well as at 24 hours post infection with VSVΔ51 at an MOI of 0.01 (CT26.WT uninfected, CT26.WT infected, CT26.lacZ uninfected, CT26.lacZ infected). The assay was performed by the Mathieu Lupien laboratory at the Princess Margaret Cancer Centre in Toronto, Canada. Histone 3 Lysine 4 dimethylation (H3K4me2) was selected as the target due to its presence being correlated with affecting chromatin structure of transcription factor binding sites (82). ChromHMM, a hidden markov model designed for processing ChIP-Seq data, was used to predict chromatin patterns of H3K4me2 in the four CT26 samples using a 10 state model (92). Each state represents a different pattern of the H3K4me2 presence or absence at 200 bp segments throughout the genome. The state for a particular location is then predicted by markov chain using probabilities derived from the ChIP-Seq peak data for each sample. The states that had patterns that differed between CT26.lacZ and CT26.WT were analyzed further by SeqPos to determine transcription factor binding motifs that matched the sites.

Supernatant Transfer

CT26.WT and CT26.lacZ cells were infected at MOI 3 with VSVΔ51-ΔG-GFP, a pseudotyped replication-competent virus that cannot produce viral G-protein and can therefore not exit the cell or produce infectious virions. After 1 hour the supernatant was aspirated and replaced with fresh media to remove any excess virus. The cells were then incubated for 24 hours at 37^{o}C and 5% CO_2. The supernatant of the infected cells was then transferred onto fresh CT26.lacZ and CT26.WT cells. For positive controls another set of CT26.WT and CT26.lacZ received 500 Units of murine IFNß, and for negative controls a set of CT26 cells received only media. The cells were incubated for 24 hours at standard conditions. Next the cells were challenged with MOI 1 wtVSV for 24 hours before being collected for plaque titering.

Western Blotting

CT26.WT and CT26.lacZ cells were cultured in 6-well tissue culture plates (~800,000 cells/well) for 24 hours before being infected with MOI 0.01 VSVΔ51. After 4, 8, 12, and 16 hours of infection, whole-cell protein extracts for western analysis were collected by the following procedure (3 technical replicate wells per time point). Wells were washed two times with cold PBS before being lysed with 200 µl of 0.1M NaF, 0.05M HEPES, 0.15M NaCl, 0.01M EDTA, 0.01M $Na_4P_2O_7$, 0.002M Na_3VO_4, protease inhibitor cocktail (Roche), 1% Triton X-100, at pH 7.4, on a rocking plate for 10 minutes at 4^{o}C. Cell lysates were collected by scraping and centrifuged at 30,100 xg at 4^{o}C for 10 minutes. Protein concentration was quantified from clarified extracts by Bradford assay (Bio-Rad Protein Assay Solution, Mississauga, ON). Twenty µg of protein were loaded into 4–12% precast gradient gels (Invitrogen) using NuPAGE SDS–

PAGE Gel system (Invitrogen), 3-(N-morpholino)propanesulfonic acid running buffer, and separated by electrophoresis at 160V for 1.5 hours. Proteins were transferred from the gel onto nitrocellulose membranes (Hybond-C, Bio-Rad) at 30 V for 2 hours at room temperature. Blots were blocked with 5% Bovine Serum Albumin (BSA) or 5% Nonfat Milk for 1 hour at room temperature, then probed for proteins of interest with 1:1000 dilution of primary antibody as described in table 1, in blocking reagent with slow shaking at 4^{o}C overnight. Blots were washed 3 times (5 minutes slow shaking each) with TBS-T (0.02M Tris Base, 0.137M NaCl, 1X Tween-20, pH 7.6) before addition of HRP-goat anti-rabbit secondary antibody for 1 hour with slow shaking at room temperature. Blots were washed again 3 times (10 minute each slow shaking) with TBS-T. Protein bands were visualized by HRP chemiluminescence (Pierce).

Table 1: Primary antibody details.

Antibody	Vendor	Catologue #	Source	Clonality	Blocking Reagent
IFNß	Antibodies-Online	ABIN1030952	Rabbit	Polyclonal	Milk
IFNAR1	Abgent	AJ1388a	Rabbit	Monoclonal	Milk
IFNAR2	LS bio	LS-C335179	Rabbit	Polyclonal	Milk
p-JAK1 (Tyr1022/1023)	Cell Signalling	3331	Rabbit	Polyclonal	BSA
Tyk2	Abnova	PAB18502	Rabbit	Polyclonal	Milk
p-Tyk2 (Tyr1054)	Aviva Systems Biology	OAEC00144	Rabbit	Polyclonal	BSA
STAT1	Cell Signalling	9172	Rabbit	Polyclonal	Milk
p-STAT1 (Tyr701)	Cell Signalling	7649	Rabbit	Monoclonal	BSA
STAT2	New England Biolabs	4597S	Rabbit	Polyclonal	Milk
p-STAT2 (Tyr689)	EMD Millipore	07-224	Rabbit	Polyclonal	BSA
IRF9	Aviva Systems Biology	ARP31200_P050	Rabbit	Polyclonal	Milk
PKA	Abnova	PAB4529	Rabbit	Polyclonal	Milk
ß-actin	Cell Signalling	4970	Rabbit	Monoclonal	Milk

Reverse Transcriptase Quantitative PCR

Total RNA was collected at various times post infection from 6-well tissue culture plates (~800,000 cells/well, 3 technical replicate wells per time point). Media was aspirated and cells were lysed, and collected using 350 µl Buffer RLT (Qiagen RNeasy Mini Kit) supplemented with 3.50 µl 2-Mercaptoethanol. Collected samples were vortexed and centrifuged at 20,000 xg for 3 minutes. Supernatants were processed following the Qiagen RNeasy Mini Kit protocol. cDNA was produced from purified RNA following the Thermo Scientific RevertAid H Minus First Strand cDNA Synthesis Kit protocol. Quantification was performed by monitoring SYBR green fluorescence every cycle after the PCR elongation step, using Applied Biosystems 7500 Real-Time PCR System.

Fluorescence Imaging

Fluorescence imaging was performed on the EVOS FL cell imaging system at 4x magnification directly in tissue culture plates. Images are false coloured for higher contrast in some cases.

High Throughput Titration

High throughput titration was performed as per the protocol outlined in Garcia et al. 2014 (100). Essentially, CT26 cells were infected for 48 hours with VSVΔ51-Fluc at an MOI of 0.01 in 96 well plates (30,000 cells/well). Twenty-five µl of the supernatant from each well was then transferred to fresh Vero cells, which are highly permissive to VSVΔ51 infection. At the same time as the transfer, a standard curve of VSVΔ51-Fluc was also added to the Vero cells ranging

from $1x10^1$ to $1x10^8$ at log intervals. Ten µl of Alamar Blue (resazurin) was added to the CT26 cells and incubated for 2 hours to indirectly estimate cell viability by metabolic activity. After 5 hours of incubation of CT26 supernatants on Vero cells, 25 µl of 2 mg/ml luciferase solution was added to each well and the plate luminescence was quantified with a standard luminometer.

siRNA

siRNA gene knockdown was performed in 96-well plates 24 hours after cell plating. In a microtube, 2.25 µl of 5 µM control scramble siRNA (Dharmacon: D-001810-01-05) or TP53RK siRNA (Dharmacon: L-061023-00-0005) was mixed with 42.75 µL serum free media. In a second tube, 1.8 µL DharmaFECT transfection reagent (Dharmacon: T-2001-01) was mixed with 43.2 µL serum free media. After 5 minutes incubation at room temperature, the solutions were combined and mixed. After 20 minutes incubation at room temperature, 360 µL of serum containing media was added to the tube. Cell culture media was aspirated prior to addition of 100 µL of siRNA mixture. Samples were incubated at 37°C in 5% CO_2 before further experimentation.

Inverse PCR

Inverse PCR was performed on CT26.lacZ purified genomic DNA. The DNA was fully digested overnight at 37°C with BfuCI (4 base cutter). BfuCI was chosen because it has a restriction site near the end of the LZSN insert sequence. PCR primers were designed to bind within the remaining end of the LZSN sequence and faced away from one another. The digested fragments

were circularized by ligation using T4 DNA ligase. Due to the orientation of the primers (facing away from each other) the amplicons produced will loop around the circularized fragment and contain the adjacent unknown genomic region to the LZSN insertion site. Amplified products were isolated by size on a 2% agarose gel and sequenced by Sanger method using the same primers as the inverse PCR. Results from sequencing were compared against the known mouse genome to identify the sites of LZSN integration.

Table 2: Inverse PCR primers.

Name	Direction	Sequence
LZSN_Fwd_3167	Forward primer	5′- TCAGGGCCAAGAACAGATGG -3′
LZSN_Rev_3054	Reverse Primer	5′- GGCCCATATTCAGCTGTTCC -3′

Results

CT26 as a model cell line for studying the characteristics of OV sensitive cells. Previous studies using Semliki VA7 identified differences in virus sensitivity between CT26.WT (resistant) and its clonal variant CT26.lacZ (sensitive). We wanted to confirm that the same could be true for VSVΔ51 in order to use these cell lines as a model to study resistance and sensitivity towards this virus as well. Indeed, Figure 1 shows that similarly to what is observed for SFV-VA7, CT26.lacZ produce over 100-fold more viral expression units (VEU: measurement relative to plaque forming units, but by luciferase reading (101)) VSVΔ51 than CT26.WT 24 hours post-infection. Using a GFP-tagged virus (VSVΔ51-GFP) to visualize spread by fluorescence microscopy, we observed that the cellular monolayer is completely infected as early as 8 hpi, whereas CT26.WT show only few foci of infection by 24 hpi (Figure 1), further highlighting this increased sensitivity of the CT26.lacZ clone towards this rhabdovirus.

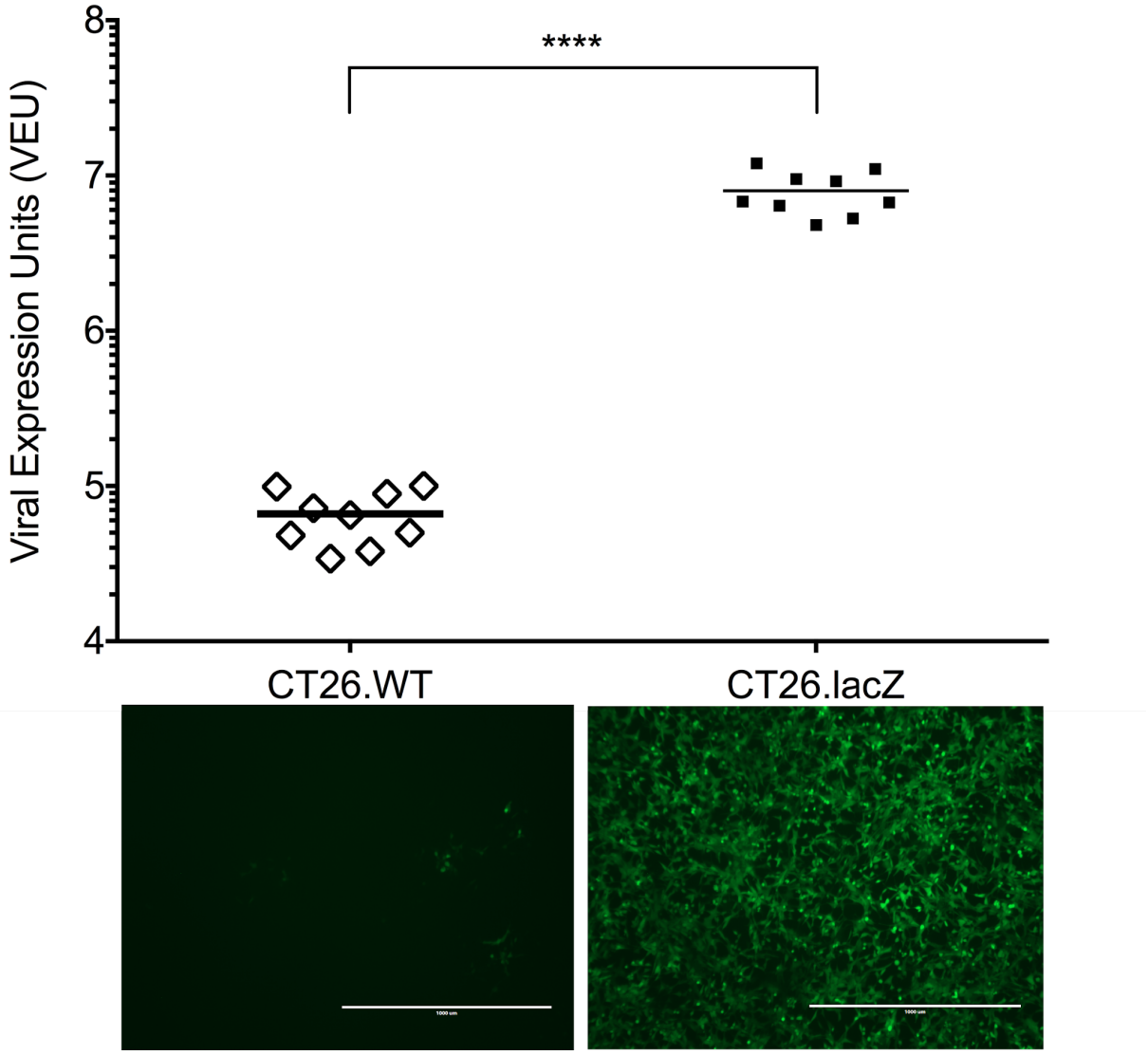
Viral Expression Units (VEU)
8
7
6
5
4
****
CT26.WT
CT26.lacZ

Figure 1: *In vitro* infection of CT26.lacZ with Oncolytic VSVΔ51 demonstrates 120 fold higher viral expression compared to CT26.WT. Confluent monolayers of CT26 (30,000 cells in 96 well dish) infected with VSVΔ51-Fluc at MOI 0.01 and titered by luciferase high throughput method (n=9) 48 hours post infection, compared by unpaired two-tailed student's t-test (**** $p<0.0001$). Fluorescence microscopy of CT26 infected with VSVΔ51 expressing GFP at MOI 0.01 24 hours post infection.

Analysis of the genomic landscape of CT26.WT and CT26.lacZ after infection with OV. The first step in our analysis was to compare the expression of genes post infection in both CT26.WT and CT26.lacZ to determine where they differ in response to a viral stimulus. The cells were infected with VSVΔ51 at a low MOI of 0.01 to allow the cells sufficient time to mount an antiviral response by the time mRNA was collected 24 hours later. Each cell line was also mock infected (i.e. received media instead of virus) and incubated for the same 24 hour period. After background correction, normalization, and summarization by RMA preprocessing, the fold change in gene expression was calculated for each cell type by calculating the difference in gene expression between the virus infected sample and the mock infected sample. Figure 2 is a heatmap of the fold change in gene expression created from the top 1% of genes with the highest fold change values. Complete-linkage euclidean-distance was used to cluster well separated round clusters of genes from one another (straight line distance from the furthest member of one cluster to the further member of another). The genes were clustered into groups based on patterns of the fold change values with CT26.lacZ on the left and CT26.WT on the right. The major clusters (determined visually) have been colour coded into groups; green, red, blue, gray, and purple.These cluster gene sets were further analyzed by gene ontology classification.

In CT26.lacZ, 748 genes were upregulated (over 2 fold) compared to 309 in CT26.WT. Many of these genes clustered into the green and gray groups which both demonstrate genes that become upregulated in CT26.lacZ post infection but remain unchanged (green) or become downregulated (gray) in CT26.WT. The genes clustered into the red group demonstrate the opposite pattern and are strongly upregulated in viral resistant CT26.WT, but show no change in CT26.lacZ. A majority of the genes in the red group were related to immune or antiviral

responses suggesting that these genes may be key in driving CT26.WT resistance to oncolytic VSV. Conversely, the lack of any upregulation or downregulation of the red cluster genes in CT26.lacZ is suggestive of a loss of function, loss of stimulus, or an inhibited pathway somewhere upstream of these genes in the CT26.lacZ cells. Because the heat map only represents the top 1% of dysregulated genes, an expanded geneset having the same gene response pattern of the red group was created using the entire microarray data set with the criteria CT26.WT −|CT26.lacZ|≥1. Upon characterising this expanded geneset into gene-ontology processes we note that all results classify as innate immune processes, and the top hit "response to IFNß" is a key determinant of VSVΔ51's tumour selective mechanism. The IFNß response pathway is typically modulated by the JAK-STAT signalling axis. Following IFNß binding to a receptor complex (IFNAR1 and IFNAR2) the signal propagates through Jak1, Tyk2, STAT1, STAT2, and IRF9 to stimulate the transcription of ISGs; the major innate antiviral genes. Hence, our microarray analysis using VSVΔ51 agrees with the results presented by Ruotsalainen et. al. who have previously shown with VA7 virus that STAT1 activation levels are very low in CT26.lacZ.

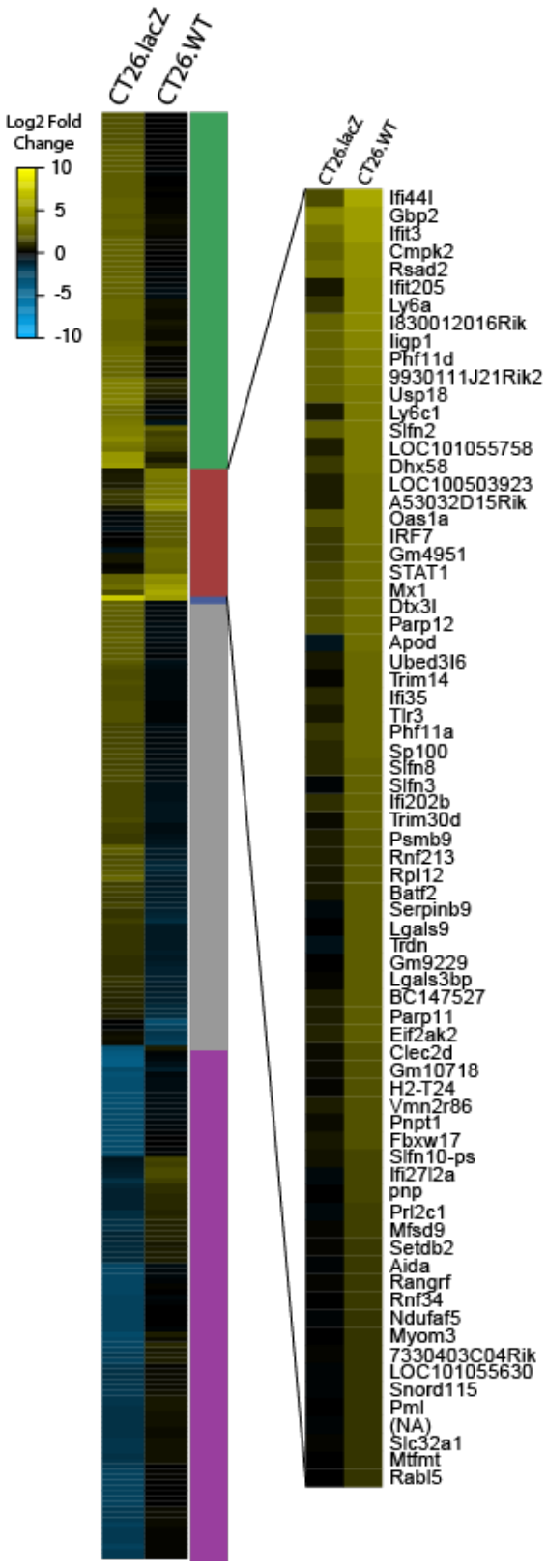
CT26.lacZ
CT26.WT
Log2 Fold Change
10
5
0
-5
-10
CT26.lacZ
CT26.WT
Ifi44l
Gbp2
Ifit3
Cmpk2
Rsad2
Ifit205
Ly6a
I830012016Rik
Iigp1
Phf11d
9930111J21Rik2
Usp18
Ly6c1
Slfn2
LOC101055758
Dhx58
LOC100503923
A53032D15Rik
Oas1a
IRF7
Gm4951
STAT1
Mx1
Dtx3l
Parp12
Apod
Ubed3l6
Trim14
Ifi35
Tlr3
Phf11a
Sp100
Slfn8
Slfn3
Ifi202b
Trim30d
Psmb9
Rnf213
Rpl12
Batf2
Serpinb9
Lgals9
Trdn
Gm9229
Lgals3bp
BC147527
Parp11
Eif2ak2
Clec2d
Gm10718
H2-T24
Vmn2r86
Pnpt1
Fbxw17
Slfn10-ps
Ifi27l2a
pnp
Prl2c1
Mfsd9
Setdb2
Aida
Rangrf
Rnf34
Ndufaf5
Myom3
7330403C04Rik
LOC101055630
Snord115
Pml
(NA)
Slc32a1
Mtfmt
Rabl5

Figure 2: Clustered heatmap analysis of the top 1% of genes with greatest fold change post infection with VSVΔ51. Yellow denotes upregulated genes post infection, blue denotes down regulated genes, and black denotes no change. Clustering performed algorithmically by complete linkage euclidean distance. Expansion shows the genes belonging to the red cluster group, which are genes highly upregulated in CT26.WT post infection that demonstrate no change in expression in CT26.lacZ.

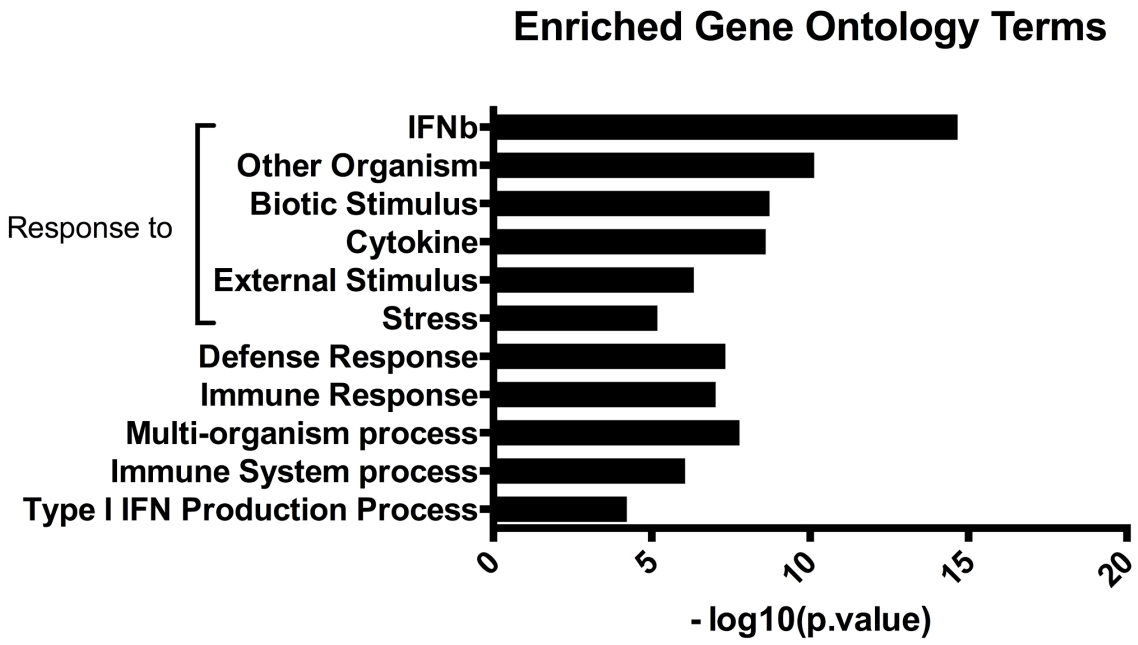
Enriched Gene Ontology Terms
Response to
IFNb
Other Organism
Biotic Stimulus
Cytokine
External Stimulus
Stress
Defense Response
Immune Response
Multi-organism process
Immune System process
Type I IFN Production Process
0
5
10
15
20
- log10(p.value)

Figure 3: Gene-Ontology analysis of unresponsive CT26.lacZ genes. Genes that are highly upregulated post infection in CT26.WT, which display no transcriptional change in CT26.lacZ, significantly participate in the above cellular processes. p-value is corrected for multiple testing using the Benjamini and Hochberg method [(p-value * number of GO terms) / i] (97, 98).

Analysis of the epigenetic landscape of CT26.WT and CT26.lacZ after infection with OV.

To complement the microarray data and to determine whether epigenetic variations between CT26.lacZ and CT26.WT were involved in the defective response to IFNß pathway, we performed whole genome epigenetic analysis by ChIP-Seq. ChIP-Seq for H3K4me2 was performed under the same conditions used in the microarray to discover differences in chromatin structure around transcription factor binding sites (TFBS). This allows for the identification of pathways that may be blocked by the epigenetic state or alternatively are not signalling and therefore not altering the epigenome around active TFBS sites post viral stimulus. In collaboration with Dr. Lupien, we applied a hidden Markov model from the software ChromHMM to create a 10 state model representing patterns of epigenomic marks observed throughout the genome (92). For example, one state may contain all locations where the chromatin was predicted as open in CT26.WT mock and virus, but closed in CT26.lacZ mock and virus based on the H3K4me2 data.

Figure 4 depicts three hypothesized patterns of potential interest for explaining differential sensitivity to viral infection: “A” for open transcription enhancer sites in CT26.WT that are closed in CT26.lacZ, “B” for transcription enhancer sites that open after viral infection in CT26.WT but are always closed in CT26.lacZ, and “C” which is the inverse of pattern “A”. A majority of the ten states created by ChromHMM account for regions where the H3K4me2 was identical in all 4 samples and had either no H3K4me2 (states 2 and 8) or complete H3K4me2 coverage (states 5, 6, 7, and 9), or where the CT26.WT and CT26.lacZ cells reacted to infection in the same manner (state 1). It fits our prediction that the cell lines should be highly similar as the CT26 cell lines are derived from the same parental cell line, hence are generally

epigenetically alike, and should only have small variations in histone marks. Hypothesized pattern “B” was not observed in any of the ten states, however, pattern “A” is present to varying degrees in states 3 and 4, and pattern C is present in state 10.

We therefore further analysed states 3,4 and 10 by performing a transcription factor motif search within the regions that these states mapped to using SeqPos software (95). Through cross filtering of the results we included only factors that were present in both states 3 and 4 and excluded any factors in state 10, considering them to be overrepresented in the genome and likely false positives. This analysis identified IRF9 as a top hit fitting these criteria. Consistent with gene expression microarray data in Figure 3 identifying the JAK-STAT pathway as a target. IRF9 is a key component of this signalling cascade as it forms the ISGF3 transcription factor complex with STAT1 and STAT2 to propagate signals in response to IFNß.

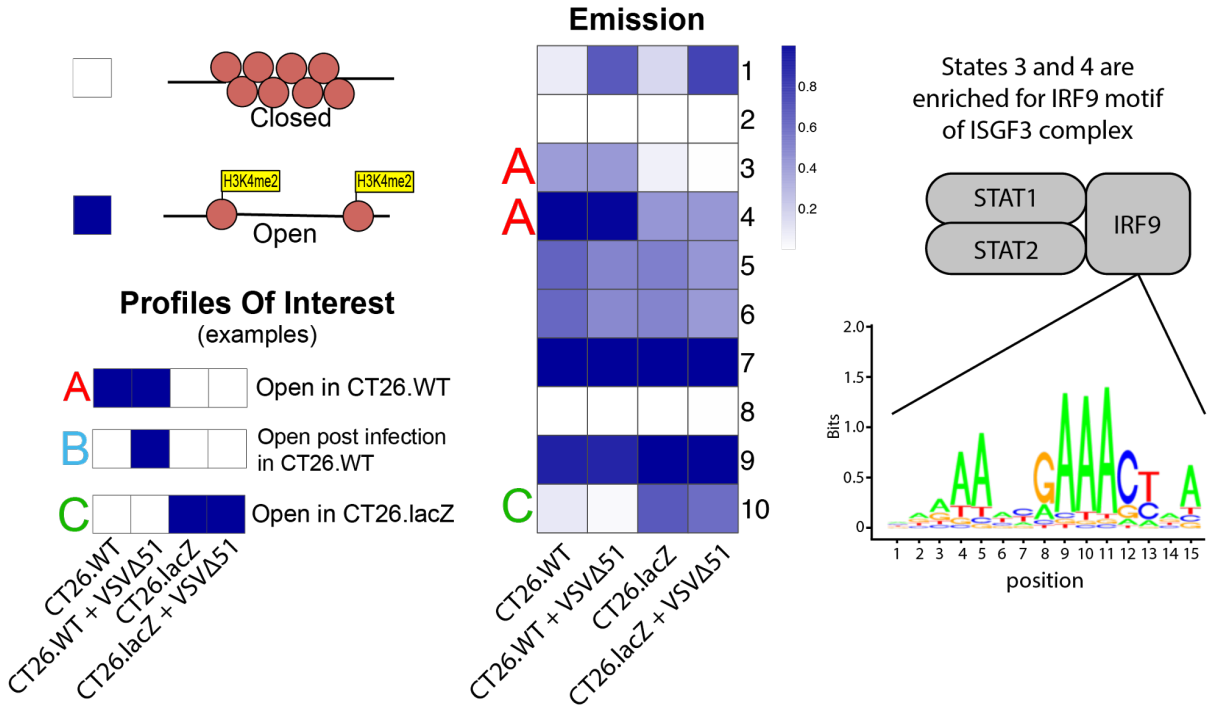
Closed
H3K4me2
H3K4me2
Open
Profiles Of Interest
(examples)
A
Open in CT26.WT
B
Open post infection
in CT26.WT
C
Open in CT26.lacZ
CT26.WT
CT26.WT + VSVΔ51
CT26.lacZ
CT26.lacZ + VSVΔ51
Emission
A
A
C
1
2
3
4
5
6
7
8
9
10
0.8
0.6
0.4
0.2
CT26.WT
CT26.WT + VSVΔ51
CT26.lacZ
CT26.lacZ + VSVΔ51
States 3 and 4 are
enriched for IRF9 motif
of ISGF3 complex
STAT1
STAT2
IRF9
2.0
1.5
1.0
0.5
0
Bits
1 2 3 4 5 6 7 8 9 10 11 12 13 14 15
position

Figure 4: ChIP-Seq analysis of transcription enhancer site histone methylation. Histone 3 Lysine 4 dimethylation analysis of CT26 subtypes with and without VSVΔ51 infection. Data was processed through ChromHMM sort genomic regions into 10 identified patterns. Hypothesis patterns A, B, and C demonstrate model patterns what we hoped to discover. States 3 and 4 matched pattern A, state 10 matched pattern C, and no states matched pattern B. Motif analysis by SeqPos of states 3 and 4 (which show patterns of open chromatin in CT26.WT and closed in CT26.lacZ) identified enrichment of the IRF9 protein that belongs to ISGF3 transcription factor complex.

CT26.WT and CT26.lacZ effectively produce IFNß following infection. As both microarray and ChIP-Seq suggested differences between CT26.WT and CT26.lacZ with respect to JAK-STAT pathway signalling upon VSV infection, we performed a more detailed examination of this signalling cascade within the resistant and sensitive cell lines. We first assayed whether the cytokine IFNß, responsible for triggering the JAK-STAT pathway, was being produced in CT26.WT and CT26.lacZ following infection with VSVΔ51.

To confirm that CT26.lacZ are transcribing IFNß mRNA upon VSV infection we performed quantitative reverse-transcription polymerase chain reaction (qRT-PCR) analysis on a time course experiment with samples collected every 4 hours post infection for 16 hours. These results show that both CT26 cell lines increase transcription of IFNß post infection, however, from 12 hpi onwards there is a significant and unanticipated increase in IFNß mRNA copies in CT26.lacZ cells compared to CT26.WT (Figure 5).

Secondly, to verify that the increased IFNß mRNA translated to increased IFNß secretion, we measured extracellular protein levels of IFNß by enzyme-linked immunosorbent assay (ELISA) at 16 hours post infection with either VSVΔ51 or Mock (Figure 5). Consistent with the mRNA transcription results, we observed that both CT26.WT and CT26.lacZ produce significant amounts of IFNß post infection, and that CT26.lacZ secrete roughly 4 times more IFNß than CT26.WT.

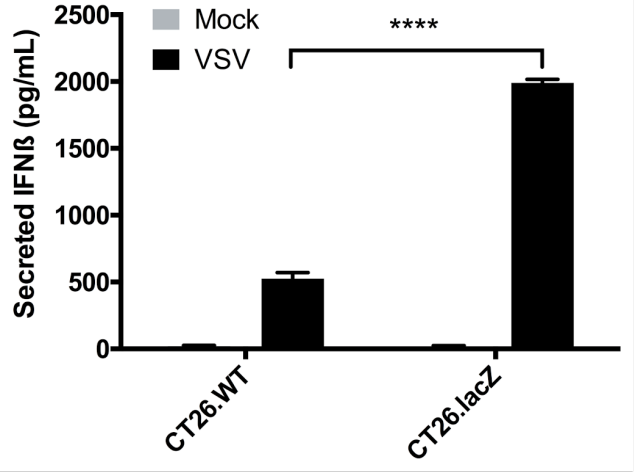
IFNß ELISA 16 h.p.i.
Secreted IFNß (pg/mL)
2500
2000
1500
1000
500
0
Mock
VSV
****
CT26.WT
CT26.lacZ

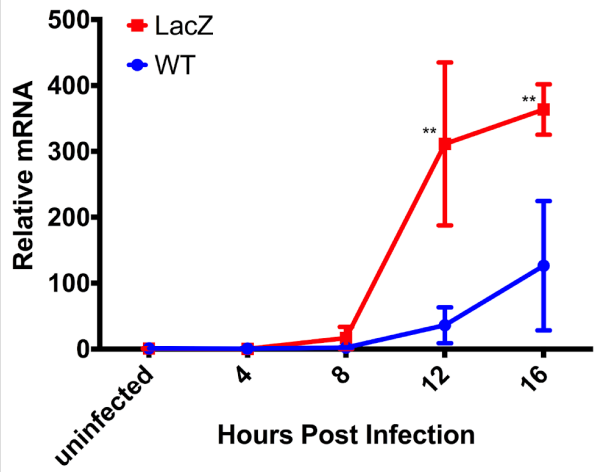
IFNß qRT-PCR
Relative mRNA
500
400
300
200
100
0
LacZ
WT
**
**
uninfected
4
8
12
16
Hours Post Infection

Figure 5: Expression and secretion of IFNß by CT26 subtypes in response to viral infection. Enzyme-linked immunosorbent assay of CT26.WT and CT26.lacZ supernatants collected 16 hours post infection with VSVΔ51 probing for murine IFNß. One-way unpaired ANOVA ($p < 0.0001$) with Tukey's honest significance difference posteriori test (**** $p < 0.0001$). Quantitative reverse transcription PCR of CT26.WT and CT26.lacZ RNA extracts collected at multiple time points post infection with VSVΔ51. Two-way ANOVA (interaction p=0.0103, sample p=0.0442, time p=0.0004) with sidak post-hoc multiple comparisons test (12h p=0.0018, 16h p=0.0054).

CT26.lacZ produce functional IFNß but cannot mount an antiviral response. These data confirmed that CT26.lacZ produce and secrete IFNß. We next determined whether IFNß from CT26.lacZ is functional, and whether CT26.lacZ can receive IFNß signals. To simultaneously address this, we performed a supernatant transfer experiment with CT26.WT and CT26.lacZ. To stimulate the release of antiviral cytokines, a first set of CT26.lacZ and CT26.WT were infected with a pseudotyped, replication-competent VSVΔ51-ΔG-GFP virus that lacks the gene to produce the viral G-protein and can therefore not exit the cell. This induces infected cells to secrete antiviral response cytokines, including IFNß, into the supernatants without releasing infectious virus. We included controls consisting of mock-infected cells (negative control) and cells to which we added exogenous IFNß (positive control). The cytokine rich supernatants were collected 24 post infection and placed on fresh CT26.WT and CT26.lacZ cells for a further 24 hours. A positive control of 500 units exogenous IFNß was also added to parallel uninfected wells at this point to activate antiviral defence pathways. At this time cells were also checked for GFP fluorescence to confirm that no VSVΔ51-ΔG-GFP had been transferred over in the supernatant (data not shown). 24 hours after supernatant transfer the cells were challenged with wtVSV at MOI 1 to determine whether each transferred supernatant could induce an effective antiviral response. In Figure 6, we can see as expected that the supernatants from mock-infected CT26.WT and CT26.lacZ cells (negative control) do not prevent infection from wtVSV. However, as observed previously with VSVΔ51, CT26.lacZ produced ~100 fold higher wtVSV titers compared to CT26.WT. Exogenous IFNß (positive control) significantly protected CT26.WT from wtVSV infection, made evident by the decreased viral titers, but was surprisingly ineffective at protecting CT26.lacZ cells. Similarly, supernatant from VSVΔ51-ΔG-

infected CT26.WT was able to significantly protect CT26.WT but not CT26.lacZ cells. Since neither exogenous IFNß nor CT26.WT cytokine supernatant could protect CT26.lacZ cells, this suggested that that the response to antiviral cytokines, and in particular to IFNß, may be defective in CT26-lacZ. To further support this, we observed that the supernatant from VSVΔ51-ΔG-infected CT26.lacZ cells was comparable to the supernatant from VSVΔ51-ΔG-infected CT26.WT cells in its ability to protect CT26.WT from wtVSV challenge. In summary, this suggests that while CT26.lacZ cells are capable of *producing* functional IFNß and antiviral cytokines capable of mounting an antiviral response, they *do not respond* to their presence.

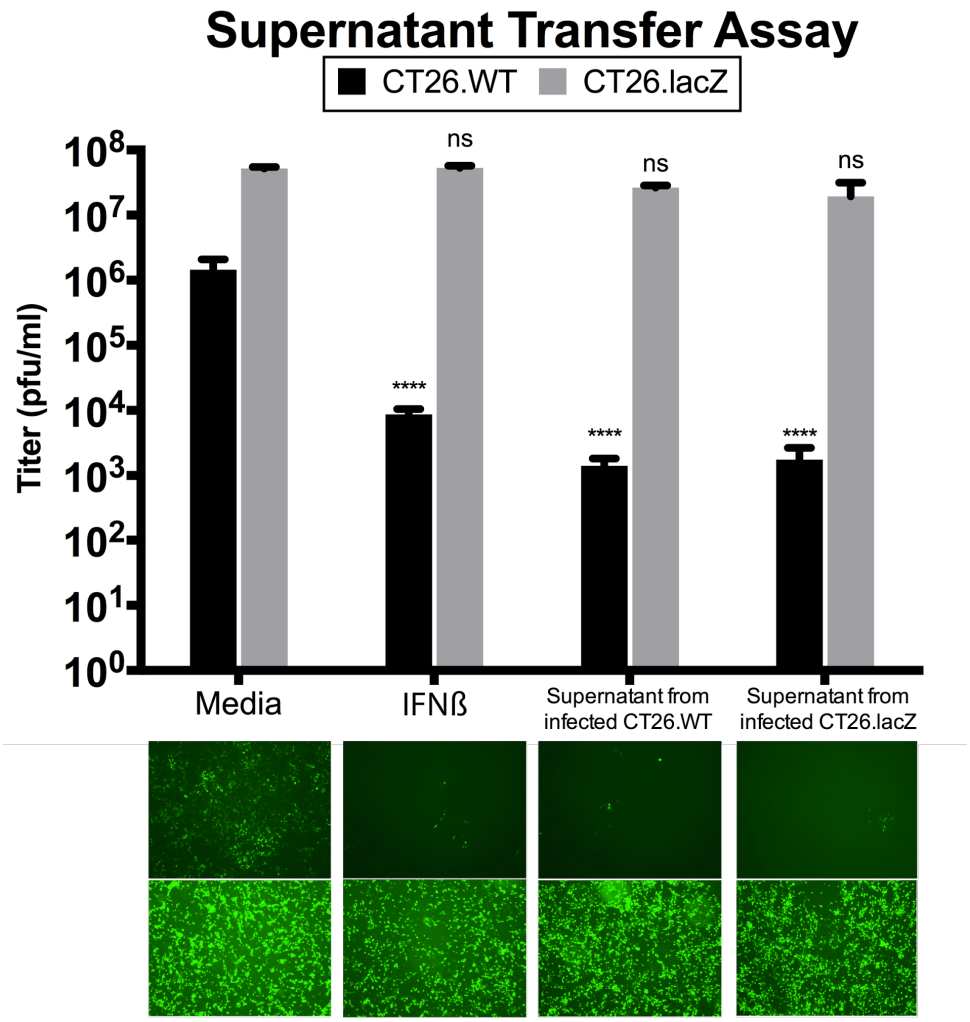
Supernatant Transfer Assay
CT26.WT
CT26.lacZ
Titer (pfu/ml)
10^8
10^7
10^6
10^5
10^4
10^3
10^2
10^1
10^0
ns
ns
ns
****
****
****
Media
IFNß
Supernatant from infected CT26.WT
Supernatant from infected CT26.lacZ

Figure 6: Supernatant transfer assay measuring CT26 subtypes production of and response to post infection cytokines. Media sample shows the expected amount of infection of both CT26.WT and CT26.lacZ by MOI 1 wtVSV. IFNß sample is the positive control exposed to 500 units of murine IFNß for 24 hours pre-infection with MOI 1 wtVSV. Experimental samples (two rightmost groups) were CT26.WT or CT26.lacZ cells infected with VSVΔ51-ΔG-GFP for 24 hours to generate supernatant which was then filtered to remove cells and transferred onto fresh CT26.WT or CT26.lacZ for 24 hours before infection with MOI 1 wtVSV. Two-way ANOVA (interaction $p<0.0001$, cell-type $p<0.0001$, pretreatment $p<0.001$) with Tukey's honest significance difference posteriori multiple comparison tests (95% CI, **** $p<0.0001$).

JAK-STAT pathway activation in response to infection is defective in CT26.lacZ cells.

To gain insight on why CT26.lacZ are unable to mount an antiviral response following conditioning with VSV-infected cell supernatants and exogenous IFNß, we examined the activation of downstream modulators of the response to type I IFN by Western blot. Proteins from whole-cell lysates were collected every 4 hours over a 16 hour period following the infection of CT26.lacZ and CT26.WT cells with VSVΔ51 at an MOI of 0.01 (Figure 7). Similarly to what was observed for IFNß mRNA and secreted IFNß, intracellular IFNß levels increased following infection with VSVΔ51 beginning at 4h and was comparable in both cell lines.

Starting at the two-component IFNAR1 / IFNAR2 membrane bound receptor complex responsible for binding extracellular IFNß, we immediately observed that CT26.lacZ produced only the immature unglycosylated 115 kDa version of IFNAR1 and contained no visible 150 kDa mature IFNAR1. The levels of immature 115 kDa IFNAR1 in both CT26.WT and CT26.lacZ are comparable, and both cell lines produced the same amount of IFNAR2.

Following IFNAR1/2 binding to type I IFN, Jak1 and Tyk2 are normally recruited and phosphorylated. However, in both CT26.lacZ and CT26.WT cells, expression and phosphorylation of Jak1 and Tyk2 was constitutive and independent of the rise in IFNß. Once phosphorylated, IFNAR1/2 bound Jak1 and Tyk2 are able to in turn phosphorylate STAT1 and STAT2, leading to their activation. Strikingly, Figure 7 shows that CT26.lacZ are nearly devoid of STAT1 and STAT2, with only very minor increases in expression over the time course. Additionally, STAT1 displayed minor activated phosphorylation, however, no activated phospo-STAT2 was observable at any time point in CT26.lacZ cells. Nevertheless, the expression levels

of these TFs even upon reaching their relative peaks, were at best equivalent to those of uninfected CT26.WT. Finally, upon examination of IRF9, which forms the transcriptionally active ISGF3 complex by binding activated STAT1/STAT2 before entering the nucleus, consistent levels of this protein were noted across all time points and in both cell lines.

Compared to western blotting, similar results were obtained looking at Jak1, Tyk2, IRF9, and STAT1/2 expression by q-RT-PCR over the same 16 hours time course with measurements every 4 hours post infection (Figure 8). Indeed, while mRNA levels of Jak1, Tyk2, and IRF9 were modestly upregulated in both CT26.lacZ and CT26.WT upon VSV infection, mRNA levels of STAT1 and STAT2 were robustly upregulated in CT26.WT (25 fold and 11 fold respectively) but not in CT26.lacZ. Altogether, these data suggest that the suppression of STAT1 and STAT2 expression/signalling in CT26.lacZ cells may lead to the inability to form the ISGF3 complex in this cell line and ultimately a block in the transcriptional upregulation of ISGs post infection.

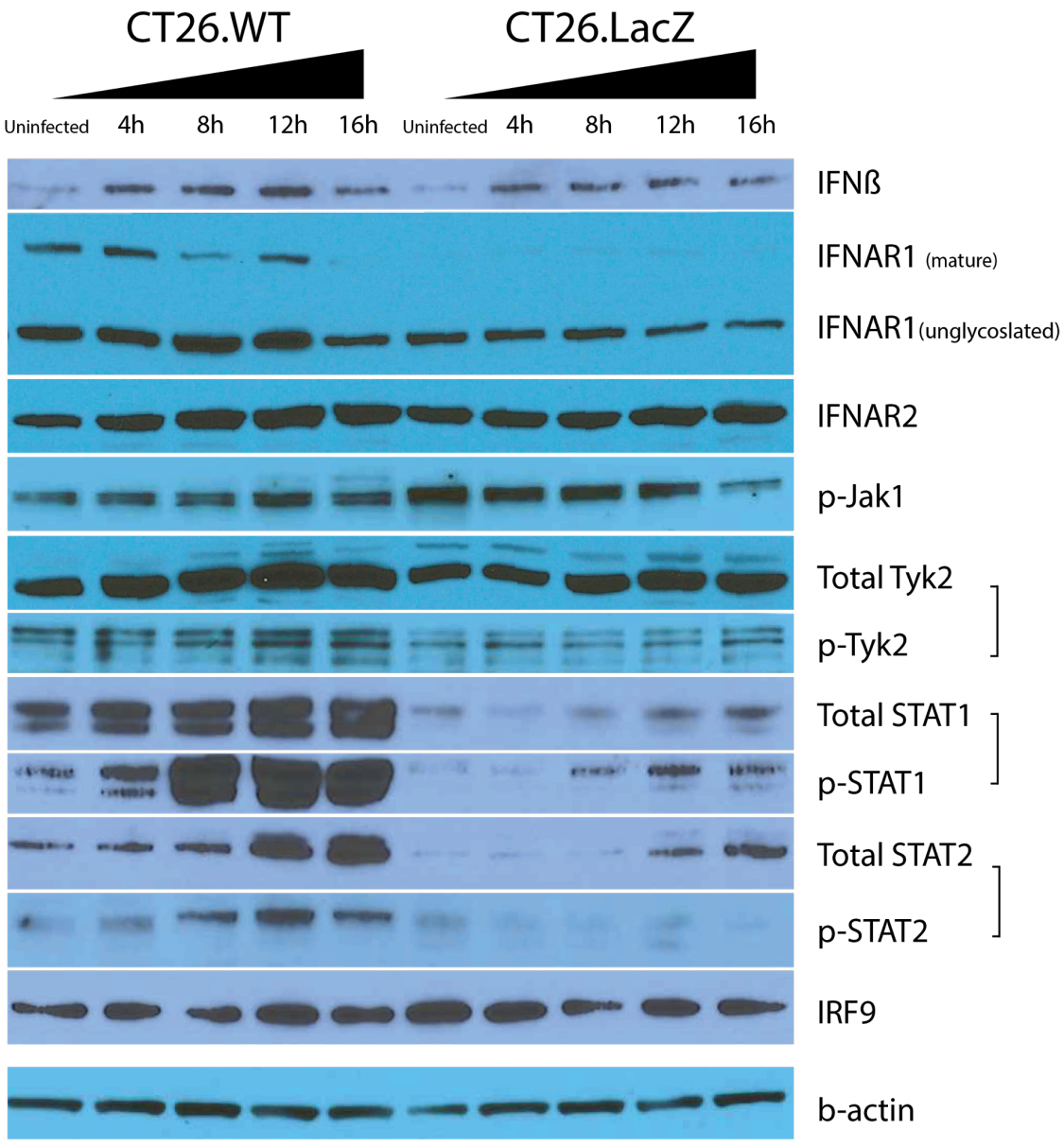
CT26.WT
CT26.LacZ
Uninfected
4h
8h
12h
16h
Uninfected
4h
8h
12h
16h
IFNß
IFNAR1 (mature)
IFNAR1 (unglycoslated)
IFNAR2
p-Jak1
Total Tyk2
p-Tyk2
Total STAT1
p-STAT1
Total STAT2
p-STAT2
IRF9
b-actin

Figure 7: Protein quantification of JAK-STAT pathway post infection in CT26 subtypes. Western blot analysis probing for components of the JAK-STAT signalling pathway in CT26.WT and CT26.lacZ where cell lysates were collected at various time points post infection with MOI 0.01 VSVΔ51. 20ug of protein per lane with ß-actin as loading control. p- denotes phosphorylated and suggests activated versions of the proteins.

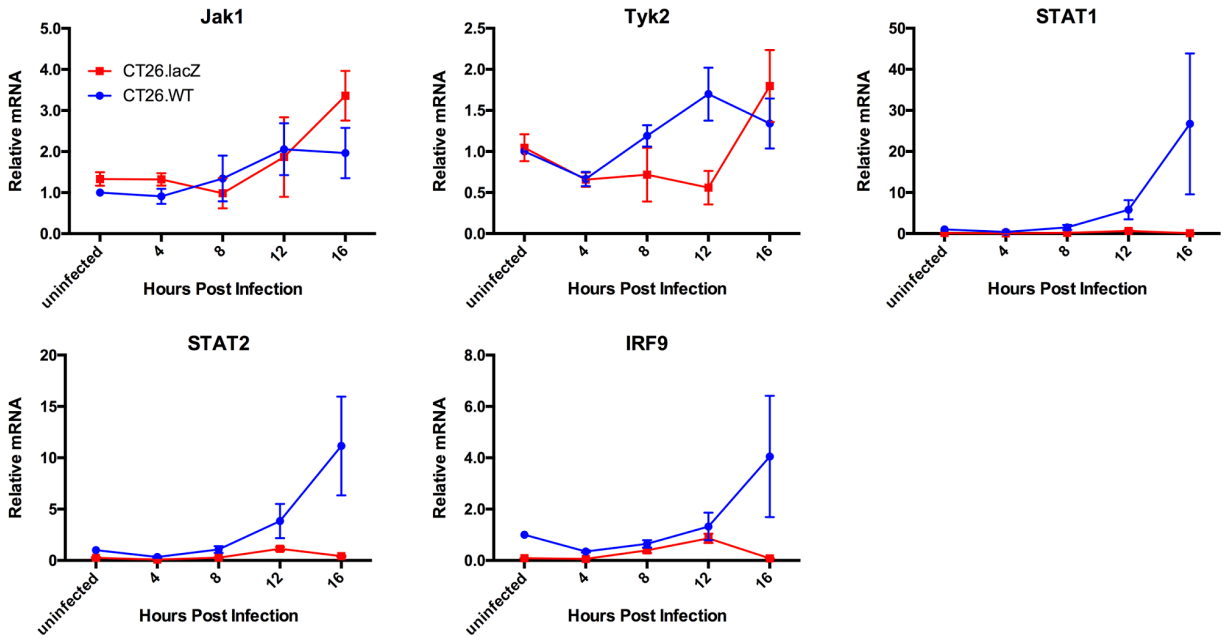
Jak1
CT26.lacZ
CT26.WT
Relative mRNA
5.0
4.0
3.0
2.0
1.0
0.0
uninfected
4
8
12
16
Hours Post Infection
Tyk2
Relative mRNA
2.5
2.0
1.5
1.0
0.5
0.0
uninfected
4
8
12
16
Hours Post Infection
STAT1
Relative mRNA
50
40
30
20
10
0
uninfected
4
8
12
16
Hours Post Infection
STAT2
Relative mRNA
20
15
10
5
0
uninfected
4
8
12
16
Hours Post Infection
IRF9
Relative mRNA
8.0
6.0
4.0
2.0
0.0
uninfected
4
8
12
16
Hours Post Infection

Figure 8: mRNA transcription levels of key JAK-STAT pathway proteins. Samples collected from CT26.WT and CT26.lacZ at various time points post infection with VSVΔ51 at MOI 0.01 (n=3, error bars display standard error of the mean). mRNA quantities are relative to the uninfected CT26.WT sample.

Genetic and Epigenetic determinants of CT26.lacZ sensitivity to oncolytic VSV.

The above data suggest that CT26.lacZ cells exhibit differences in sensitivity to oncolytic VSV due to their inability to mount an effective antiviral response, linked to the lack of expression and induction of STAT1/2 as compared to CT26.WT. We considered two non-mutually exclusive hypotheses that could explain this observation:

i. The single cell isolation step during the process of developing CT26.lacZ has led to the selection of an epigenetically more sensitive subclone of the CT26.WT population.
ii. The inserted LZSN vector used to transduce the lacZ gene has inserted in the CT26 genome and caused a mutation within a key antiviral response gene or regulatory element.

Isolated CT26.WT subclones exhibit heterogenous sensitivity to infection with VSVΔ51.

To test the first hypothesis we isolated 21 single cell subclones of CT26.WT by limiting dilution. Each clone was then tested for its sensitivity to VSVΔ51-luciferase infection at an MOI of 0.01 for 48 hours, as determined by virus output (using a high-throughput assay (100)) and viability using Alamar Blue, a resazurin-based metabolic dye (Figure 9). Remarkably, CT26.WT subclones exhibited a wide range of sensitivity to VSVΔ51, with the most sensitive subclones producing over 100-fold more virus than the most resistant subclones. However, despite this wide range, no subclones reached the viral output of CT26.lacZ, which was roughly another 100 fold more sensitive than the most sensitive CT26.WT subclone. Using lognormal distribution which best fit the sensitivity data of CT26.WT population, we estimated the probability of selecting a CT26.lacZ-like clone to be 0.00076%, or roughly 1 in every 131,000 subclones.

While this does not fully exclude the possibility that the high sensitivity of the CT26.lacZ line is due to random chance, this argues in favour of the possibility that retroviral insertion could be at the root of the observed super-sensitivity.

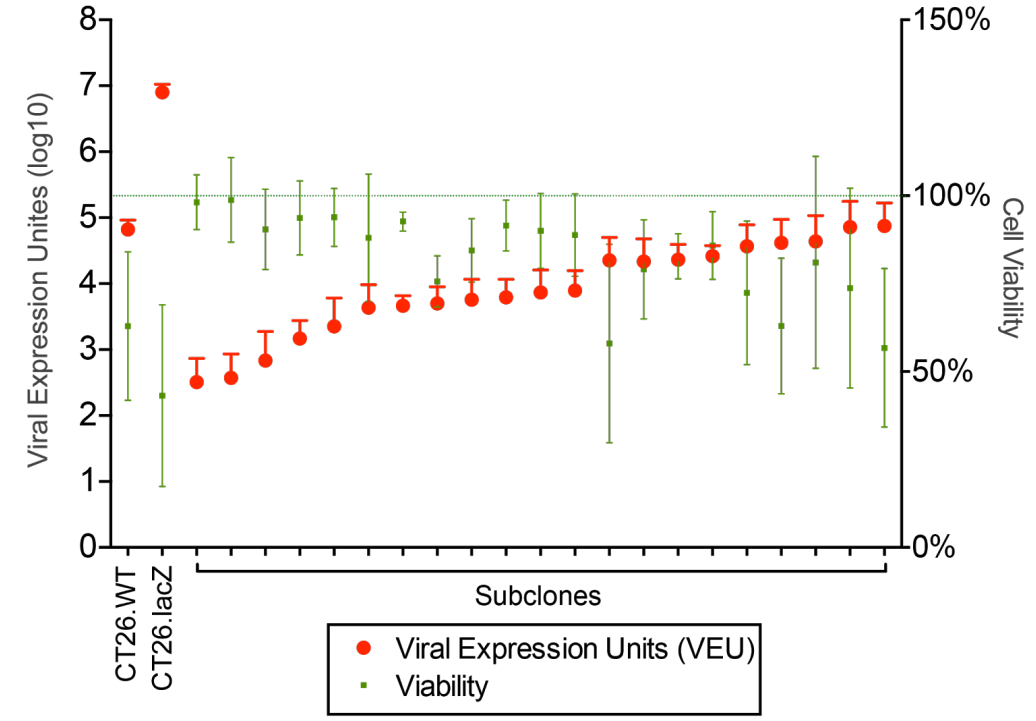
Viral Expression Unites (log10)
Cell Viability
8
7
6
5
4
3
2
1
0
150%
100%
50%
0%
CT26.WT
CT26.lacZ
Subclones
Viral Expression Units (VEU)
Viability

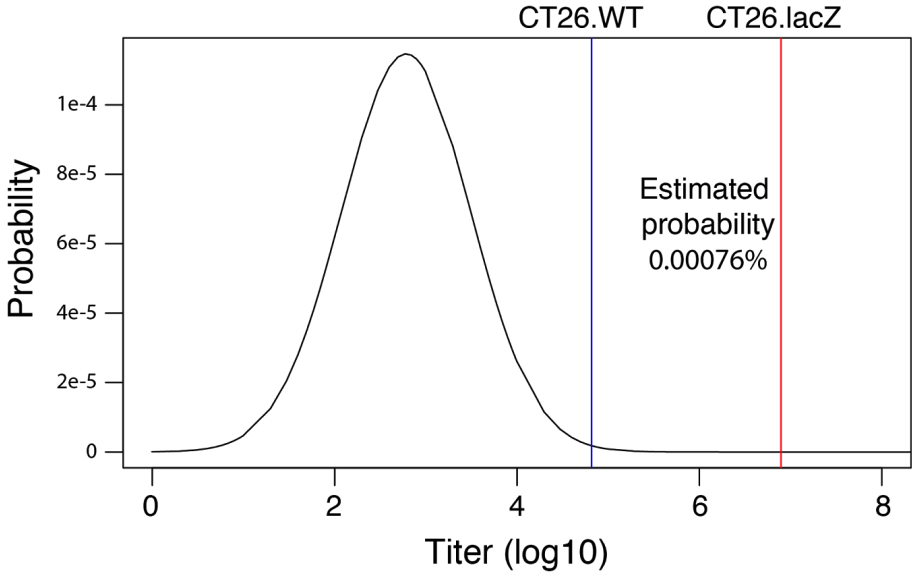
CT26.WT
CT26.lacZ
Probability
1e-4
8e-5
6e-5
4e-5
2e-5
0
Estimated
probability
0.00076%
0
2
4
6
8
Titer (log10)

Figure 9: Heterogeneous sensitivity to VSVΔ51 infection of isolated CT26.WT subclones. Viral sensitivity analysis of 21 subclones isolated from CT26.WT cell line. Cells were infected with VSVΔ51-Fluc at an MOI of 0.01 for 48 hours before titration by high throughput luciferase and viability assay by Alamar Blue (3 technical replicates each with 3 biological replicates, total n=9). Probability analysis of log-normal distributed data estimates a probability for discovering a subclone having the sensitivity of CT26.lacZ based on the 21 subclone profile.

Identification of Genomic integration sites of the LZSN vector in CT26.lacZ. Given that the retroviral insertion sites of the CT26.lacZ were unknown, we performed inverse PCR on CT26.lacZ genomic DNA using primers designed to recognize the known sequence of the retrovirally inserted LZSN vector. This approach would allow for the identification of LZSN integration sites within the CT26.lacZ genome following restriction enzyme digestion, fragment self-ligation, LZSN-primer-based amplification, and amplicon sequencing. Amplicons produced by the inverse PCR method were first isolated by electrophoresis on 2% agarose gels, from which we observed multiple bands of varying sizes suggesting multiple integration sites (Figure 10). The bands were individually cut out and sequenced by Sanger capillary sequencing and compared against the known mouse genome to identify the locations of LZSN insert sites. Table 3 shows the closest gene associated with each integration site. A Kinase Anchoring Protein 7 (AKAP7) has an LZSN sequence facing in the reverse transcriptional direction of the genes within the third intron. TP53 Regulating Kinase (TP53RK) has an LZSN sequence in the same transcriptional orientation as the TP53RK gene located in the first intron of the gene. XR_383903.1 has an LZSN sequence in the same transcriptional orientation located 476 bp upstream, however the gene itself is a pseudogene with no likely function. A fourth integration site was also found, however it appears to be quite far from any expressed gene, the closest being SMAD1 at 155,000 bp away.

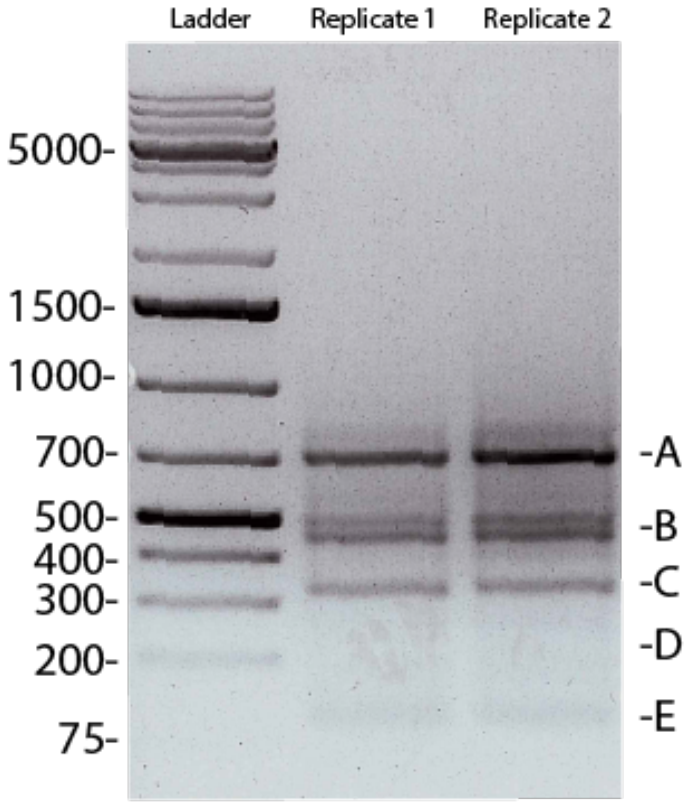
Ladder
Replicate 1
Replicate 2
5000-
1500-
1000-
700-
500-
400-
300-
200-
75-
-A
-B
-C
-D
-E

Figure 10: LZSN integration sites in the CT26.lacZ genome gel electrophoresis. CT26.lacZ genomic DNA digested with BfuCI overnight. Digested DNA was circularized by T4 DNA ligase and PCR amplified by inverse PCR primers. The resulting amplicons were separated on a 2% agarose ethidium bromide gel to separate different integration sites. Major bands are labelled A through E and were isolated for sequencing.

Table 3: Identification of genes closest to LZSN integration sites in CT26.lacZ. Sequenced Integration sites mapped to genomic locations in the known mouse genome.

Gene	Distance to transcription start site (bp)	Annotation
AKAP7	25,596	Third Intron
Tp53rK	614	First Intron
XR_383903.1	-476	None
Smad1	-155,000	None

Investigation of AKAP7. AKAP proteins are responsible for the localization of protein kinase A (PKA) to specific cellular compartments and help to anchor the kinase near its target proteins. Up to 15 different AKAP family proteins are expressed in mammalian cells, each directing the activation/inhibition of various cellular processes (102). AKAP7 protein is expressed as two short isoforms designated AKAP7α and AKAP7ß that are membrane localized, and two long isoforms designated AKAP7δ and AKAP7γ that are found in the nucleus (103). All isoforms of AKAP7 contain an RII domain that binds protein kinase A for subcellular localization (103). As the LXSN vector insert was located in the third intron of AKAP7 we deemed it possible that expression of the long isoforms of AKAP7 may be inhibited. We assessed mRNA levels of the long AKAP7γ isoform and the short AKAP7ß isoform by qRT-PCR using primers targeting exons unique to each form (Figure 11). Consistent with what was expected, CT26.lacZ transcribe roughly 40% less mRNA for the long form AKAP7γ in comparison to CT26.WT. Furthermore, CT26.lacZ transcribed roughly 2.5 fold more mRNA of the short membrane localized AKAP7ß isoform. The mRNA ratio of AKAP7 isoforms in CT26.lacZ is highly skewed possibly due to LXSN vector integration within the gene.

To assess whether changes in expression of AKAP7 isoforms can affect the cellular sensitivity to viral infection, we overexpressed AKAP7ß-GFP or AKAP7γ-GFP by transfecting expression vectors into cells. Overexpression of AKAP7 variants was performed in 293T cells, as the AKAP7-GFP vectors expressed the human proteins, and also due to the high transfection efficiency of the 293T cell line. In mock transfected GFP only vector we observe a titer of $7.7x10^7$ pfu after 48 hours of infection with VSVΔ51 in 293T cells (Figure 11). As predicted, overexpression of AKAP7ß isoform led to an increase in viral titers (specifically, 2.8 fold), and overexpression of AKAP7γ lead to very potent suppression of viral infection leading to an 11.2 fold decrease in overall viral titers. In conclusion, this data suggests that a disturbance to the normal ratio of AKAP7 isoforms in CT26.lacZ caused by the integration of LXSN into the third intron may play a major role in the cellular sensitivity to viral infection.

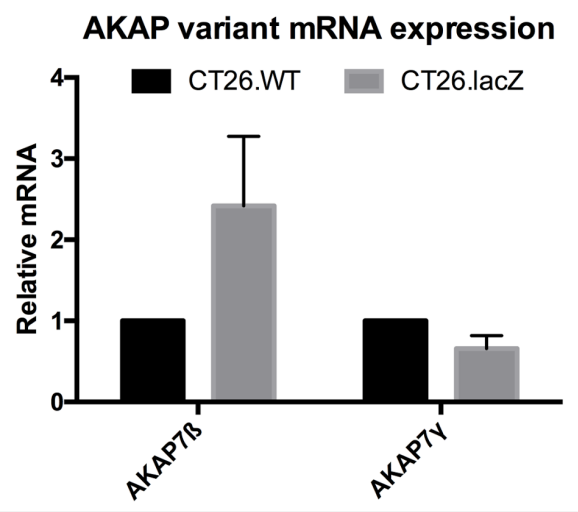
AKAP variant mRNA expression
CT26.WT
CT26.lacZ
Relative mRNA
4
3
2
1
0
AKAP7ß
AKAP7γ

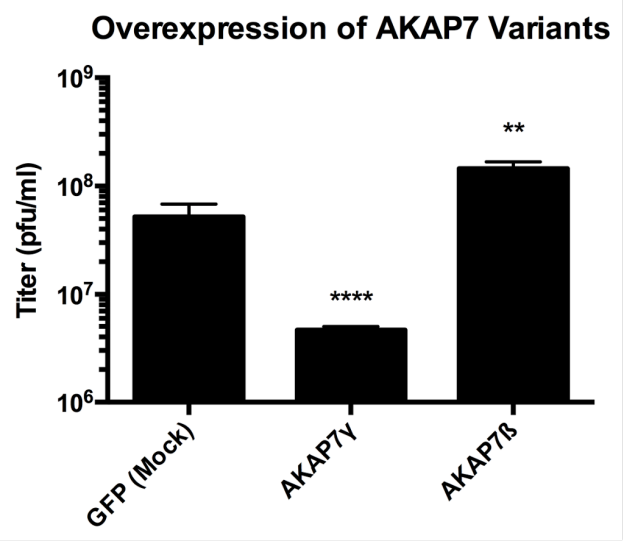
Overexpression of AKAP7 Variants
Titer (pfu/ml)
10^9
10^8
10^7
10^6
****
**
GFP (Mock)
AKAP7γ
AKAP7ß

Figure 11: Comparison of AKAP7 variant expression and effect on sensitivity of infection in CT26WT and CT26.lacZ. Left panel: Quantitative reverse transcription PCR of AKAP7ß and AKAP7γ in CT26.WT and CT26.lacZ in uninfected cell cultures. Right panel: Titers of human 293T transfected with gene expression vectors overexpressing either AKAP7ß or AKAP7γ after 48 hours if infection with VSVΔ51-GFP, One way ANOVA ($p < 0.0001$) with post-hoc Dunnett's multiple comparisons test (** $p < 0.01$, **** $p < 0.0001$).

Investigation of TP53RK. To determine if the LZSN insert had any transcriptional effect on TP53RK expression we measured mRNA transcripts by qRT-PCR in both CT26.WT and CT26.lacZ and observed a 75% reduction in TP53RK expression in CT26.lacZ. To test whether the reduction in TP53RK was able to affect cellular sensitivity to viral infection we performed an siRNA knockdown of TP53RK and compared to a control scramble siRNA. Cells were transfected for 24 hours before infection with VSVΔ51 at an MOI of 0.01. The results show that TP53RK knockdown increased viral titers by 6.7 fold. Overall, this suggests that TP53RK participates in the cellular resistance to VSV infection and that it may be connected to the antiviral response defects observed in CT26.lacZ, albeit through a mechanism that remains elusive.

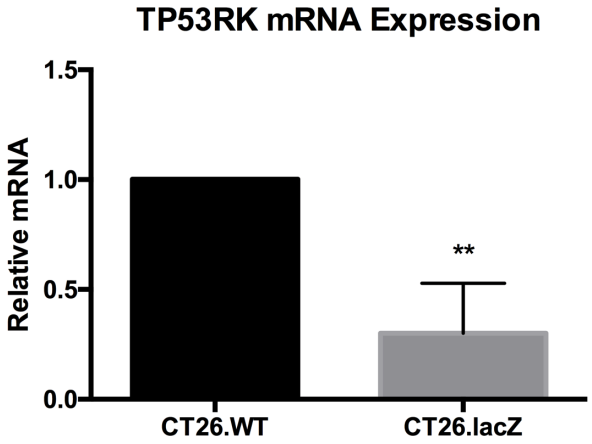
TP53RK mRNA Expression
Relative mRNA
1.5
1.0
0.5
0.0
**
CT26.WT
CT26.lacZ

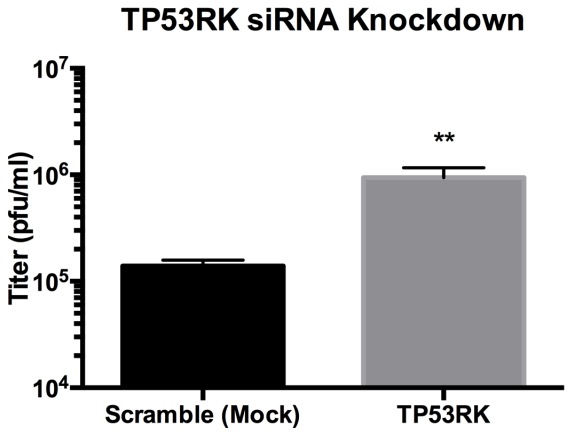
TP53RK siRNA Knockdown
Titer (pfu/ml)
10^7
10^6
10^5
10^4
**
Scramble (Mock)
TP53RK

Figure 12: TP53RK transcript expression and siRNA knockdown in CT26.WT and CT26.lacZ. Top panel: Quantitative reverse transcription PCR of TP53RK mRNA expression in CT26.WT and CT26.lacZ uninfected cells. Bottom panel: Knockdown of TP53RK by siRNA transfection followed by infection with VSVΔ51-GFP at an MOI of 0.01. Unpaired two-tailed student's t-test (n=3, ** $p < 0.01$).

Discussion

The investigation of CT26.lacZ sensitivity to viral infection has led to the discovery of a previously unknown connection between both AKAP7 and TP53RK permissiveness to VSV infection and potentially to the regulation of the JAK-STAT antiviral response pathway.

Microarray data analysis identified differences in the response to IFNß process resulting from the failure to activate transcription of ISGs in CT26.lacZ cells compared to CT26.WT. This observation is in agreement with the findings of Ruotsalainen et. al. who observed a suppression of STAT1 activation in CT26.lacZ cells upon VA7 infection — STAT1 being a key component of response to IFNß. Interestingly, in the microarray data, roughly 2.5 times more genes were upregulated in CT26.lacZ compared to CT26.WT upon VSV infection, likely due to the sensitivity of LacZ to virus infection. To control for the latter, we applied clustering gene expression data to isolate groupings of genes based on expression patterns. This was key in filtering out relevant genes related to the viral sensitivity phenotype from the large amount of background of genes acting in alternative defence pathways, stress pathways, apoptosis, and necrosis.

ChIP-Seq data further confirmed this finding by highlighting that CT26.lacZ had closed chromatin structure in many TFBS that were open in CT26.WT, and that these sites were enriched for the TFBS of JAK-STAT transcription factor complex ISGF3, which is responsible for the activation of ISGs. Because ISGF3 is known to function with Histone acetyltransferases and other epigenetic modifiers, it is unclear whether these epigenetic changes are the cause of sensitivity or a result of the lack of upstream signalling from the JAK-STAT pathway (39-41).

Starting at the top of this pathway, we first confirmed that CT26.lacZ were able to secrete functional IFNß that can properly elicit protection from viral infection. Furthermore, we confirmed that CT26.lacZ cells were unable to trigger a cellular antiviral state when pretreated with secreted antiviral cytokines including exogenous IFNß. These results taken together suggested that in VSV-sensitive CT26.lacZ cells, the JAK-STAT signalling pathway has been rendered defective.

Therefore, we quantified the protein levels of each component in the JAK-STAT canonical pathway by western blot. As we suspected, this analysis revealed dysregulation in the expression of several JAK-STAT pathway proteins in CT26.lacZ.

Firstly, we probed cell lysates for IFNAR1, the JAK-STAT membrane receptor that is responsible for initiating JAK-STAT signal propagation in the presence of extracellular IFNß. Active (or mature) IFNAR1 is post translationally modified by multiple glycosylation sites on the extracellular region that cause the protein to be more than twice its expected size, and therefore visible at 150 kDa in CT26 cells (104). CT26.WT displayed high levels of the mature 150 kDa IFNAR1, from the mock infected samples up to 16 hours post infection, at which point mature IFNAR1 protein was mostly gone, potentially due to the negative feedback of the pathway causing removal of the receptor from the membrane and degradation of IFNAR1 (42). In CT26.lacZ cells, mature 150 kDa IFNAR1 was not expressed at any of the time points assayed. Interestingly, both CT26.WT and CT26.lacZ express equal levels of the immature 115 kDa IFNAR1 protein. Unglycosylated IFNAR1 is not expected to participate in any type I IFN signalling, however, the consistent expression of the protein in both cells lines suggests that

CT26.lacZ are able to properly translate IFNAR1, and that the glycosylation/maturation process or a regulator of mature IFNAR1 recycling/degradation is instead the cause of inhibition.

Secondly, the kinase Tyk2 is recruited to the cytoplasmic tail of mature IFNAR1 where it scaffolds and mediates phosphorylation of STAT2 (34, 35). Tyk2 phosphorylation occurs independently of IFNAR1 activation (35), and as such, we observed equal levels of phosphorylated Tyk2 protein in both CT26 cell lines.

Thirdly, STAT2 activation requires activated membrane bound IFNAR1 in addition to phosphorylated Tyk2 to initiate recruitment of STAT2 for phosphorylation at the receptor complex. Therefore, because we have already identified that CT26.lacZ have no mature IFNAR1 we expected and observed no phosphorylated STAT2 pre or post infection with VSVΔ51. Furthermore, this observation supports that the immature 115 kDa IFNAR1 is not participating in STAT2 activation or type I IFN signalling.

Finally, phosphorylation of STAT1 is performed by Jak1 kinase bound to the cytoplasmic tail of IFNAR2, however, it requires IFNAR1, Tyk2, and STAT2 activation to occur first which scaffold and recruit STAT1 to the receptor complex for phosphorylation. Therefore, once again because CT26.lacZ have no mature IFNAR1 or phosphorylated STAT2, we expect the levels of STAT1 phosphorylation to also be inhibited. As expected, the CT26.lacZ samples have dramatically lower levels of STAT1 phosphorylation compared to CT26.WT. However, despite the complete abrogation of phosphorylated IFNAR1 and phosphorylated STAT2, we still observe a small amount of STAT1 phosphorylation, possibly suggesting that Jak1 and IFNAR2 are functional, yet performing at very low efficiency.

In addition to these findings, we must also note that the baseline total STAT proteins are much lower in CT26.lacZ compared to CT26.WT cells. We hypothesize that this is likely caused by the long term inhibition of IFNAR1 maturation and subsequent inhibition of STAT activation slowly leading to overall lower levels of STAT proteins in CT26.lacZ cells over time. We currently do not know whether IFNAR1 inhibition alone is enough to induce the virus sensitive phenotype, or whether the loss of STAT protein expression is required to reach optimal sensitivity.

Two hypotheses were proposed to explain the absence of mature IFNAR1 in CT26.lacZ cells. The first hypothesis was that single cell isolation of CT26.lacZ during the creation of the cell line selected for a more sensitive subclone from the CT26.WT population. Because CT26.WT were pre-subcloned to reduce heterogeneity before undergoing the process of inserting lacZ, any heterogeneity within the cell line would need to have developed post CT26.WT subcloning and may possibly be epigenetic in nature (71). We suspected that during the creation of CT26.lacZ, Wang et. al.'s selection of the highest ß-galactosidase producing subclone may have unintentionally biased for the selection the most sensitive subclone to viral infection, which allowed for high rate of retroviral infection/transduction. However, after testing this hypothesis through subcloning of CT26.WT and assaying the sensitivity of every isolated clone, we in fact discovered that while the CT26.WT cell line does demonstrate heterogeneity in response to viral infection, most subclones were actually more resistant than the overall population, and no subclones were close to the sensitivity of CT26.lacZ. Furthermore, the CT26.WT subclone sensitivity "drifted" when passaged repeatedly over time (data not shown), whereas CT26.lacZ always presented a stable and very consistent VSVΔ51 output titer of ~1e7 pfu. Due to these

findings we decided to test the hypothesis that that the LZSN vector inserted into the CT26 genome caused a mutation within a key antiviral response gene or regulatory element.

Identifying sites of lacZ insertion by inverse PCR we identified 4 integration sites in the genome with two sites occurring in gene coding regions.The first gene coding integration site was in AKAP7. AKAP proteins are well documented for localizing PKA into specific cellular compartments thereby directing activation or inhibition of cellular processes. AKAP7 has been studied in the context of calcium channel regulation, however its cellular function is poorly documented compared to other AKAP family proteins. It is known that AKAP7 exist as 4 major variants with two short membrane localizing variants, and two long nuclear localizing variants (49). No link has been made between AKAP7 and the JAK-STAT pathway, however, several separate studies not involving AKAP7 have reported that PKA activation leads to potent inhibition of the JAK-STAT signalling cascade (105-109). In 1996 David et al. demonstrated that activation of PKA by forskolin led to tyrosine phosphorylation of IFNAR1 resulting in inhibition. Interestingly the authors also observed an eventual reduction of STAT1 and STAT2 protein levels (109). Considering that these observations align with those of CT26.lacZ and that AKAP7 is a known PKA chaperone, we propose that AKAP7 may be a previously unknown regulator of type I IFN by controlling the localization of PKA through long and short variants to modulate inhibition of IFNAR1. In CT26.lacZ, the LZSN vector has inserted into the third intron of AKAP7 and faces in the opposite direction of AKAP7 transcription. We measured the mRNA expression of long variant AKAP7γ and the short variant AKAP7ß in both CT26 cell lines, and observed that CT26.lacZ expressed roughly 40% less AKAP7γ and 2.5 fold more AKAP7ß compared to CT26.WT. AKAP7 has three known transcription start sites, two of which drive the

long variants and a separate start site located after the 6th intron that drives the transcription of both short variants. Therefore, it is possible that LZSN insertion is disrupting transcription of only the long variants AKAP7δ/AKAP7γ through splice defects or promoter interference, and not affecting transcription of the short variants due to the distance from the insert to AKAP7ß/ AKAP7α transcription start site (Figure 13).

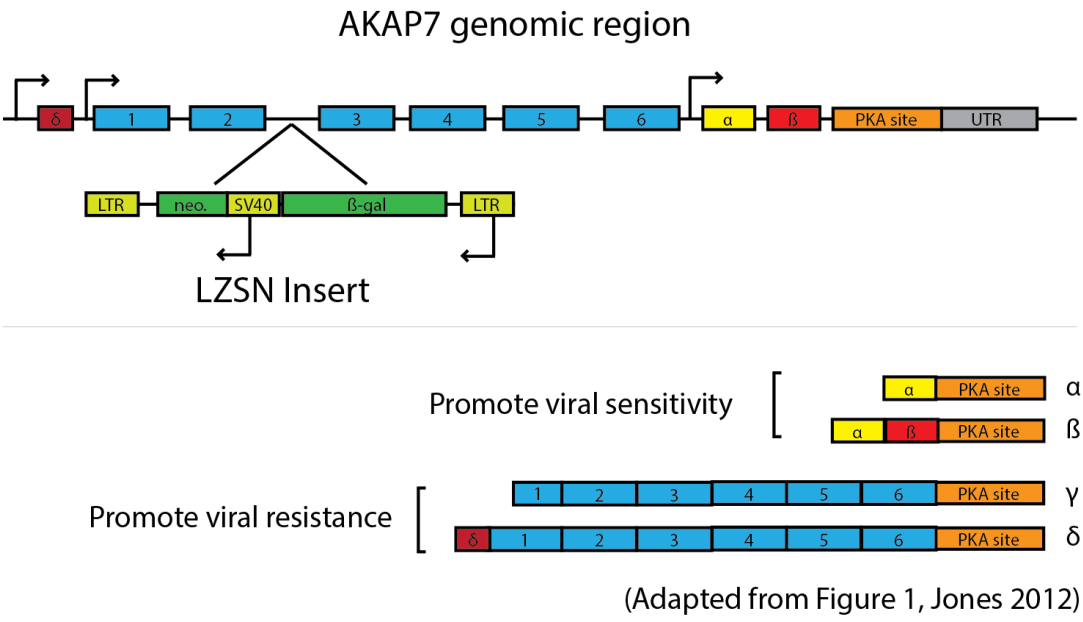

Figure 13: Illustration of AKAP7 variants and LZSN integration site in CT26.lacZ. Exon map adapted from Figure 1 of Jones 2012 showing the integration site of LZSN in CT26.lacZ

(103). The bottom section shows the four major variants and their hypothesized effects on viral sensitivity/resistance.

While David et al. did not identify the specific residue phosphorylated by PKA, we hypothesize that the short membrane localizing AKAP7ß/AKAP7α promote IFNAR1 inhibition

by proximity PKA-mediated phosphorylation of tyrosine 481, 527, or 538 of the cytoplasmic portion of IFNAR1, thus catalyzing Tyk2 phosphorylation of serine 535 which has been well documented to lead to IFNAR1 ubiquitination and lysosomal degradation (42). Therefore, by simply changing the ratio of AKAP7 variant expression, cells could precisely tune the regulation of type I IFN response allowing them to limit over-inflammation and to reset the signalling pathway. In fact, we also performed western blot analysis probing for PKA, using the same samples that were used to measure the JAK-STAT components. We observed that CT26.WT expressed almost no PKA pre-infection, but gradually expressed more as time passed post infection, and seemed to inversely correlate with the inhibition and loss of mature IFNAR1 (Appendix: supplemental 2). Furthermore, CT26.lacZ never produced mature IFNAR1, possibly due to the high levels of PKA expressed at all time points, including pre-infection (Figure 7). By overexpressing AKAP7γ or AKAP7ß in 293T cells we were able to manipulate the viral sensitivity of the cells. It is to be noted that because 293T cells are naturally much more sensitive than CT26.WT, the cells are already likely close to viral production saturation, and therefore we did not expect to see the 100 fold increase in titer observed in CT26.WT to CT26.lacZ. Nonetheless, AKAPß overexpression successfully increased viral output leading to 2.8 fold increased viral titers. Surprisingly, AKAP7γ overexpression led to strong viral resistance and decreased titers by 11.2 fold. Originally we had assumed that AKAP7γ nuclear localization may simply sequester PKA away from IFNAR1, but did not expect it to also induce a more resistant state. This brings forth the possibility that nuclear AKAP7/PKA has an active opposing role that enhances components of type I IFN response. Interestingly, most AKAPs only bind type II PKA, however, AKAP7δ/AKAP7γ are the first nuclear localized AKAP that can also bind type I PKA

(59, 110). Future experimentation should explore these details and also probe the existence of an AKAP7 mediated transcriptional machinery activation/inhibition role that may contribute to the downregulation of STAT1 and STAT2 expression in CT26.lacZ.

The second integration site of interest is within the first intron of TP53RK, an activating kinase that phosphorylates serine 15 of Tumour Protein p53 (p53) (111, 112). p53 is the central transcriptional regulator of multiple pathways that manage cellular health, such as cell cycle, apoptosis, autophagy, and senescence (25). Mutations in p53 gene are common driver mutations in cancer cells, present in over 50% of human cancers [24]. CT26, however, are known to express functional p53 [113]. Phosphorylation of serine 15 stabilizes and activates p53 by altering the conformation of one of its alpha helixes to block E3 ubiquitin ligase MDM2 from binding and degrading p53 (114). Many studies have shown that p53 accumulation and activation plays an antiviral role in cells, mainly through the rapid initiation of apoptosis that impedes virus replication (25). As described in the introduction, p53 knockout cells fail to activate apoptosis under viral stress, which results in much higher titers of VSV (47), and many viruses have developed mechanisms that allow them to manipulate cellular p53 by either inhibiting the activation of p53 or promoting p53 degradation (25). Takaoka et al. 2003 outlined that p53 expression is upregulated post IFNß signalling, but also noted that phosphorylation of serine 15 occurs independently of type I IFN (47). While the kinases responsible for serine 15 phosphorylation in response to DNA damage have been well characterized, no detailed mechanism is known to explain activation of p53 post viral stress. CT26.lacZ cells express roughly 75% less TP53RK compared to CT26.WT supporting that the integration of LZSN is detrimental to TP53RK expression in CT26.lacZ. Additionally, we performed siRNA knockdown

of TP53RK in CT26.WT in an attempt to recreate CT26.lacZ phenotype and observed almost a 1 log increase in viral titers. Therefore, we propose that TP53RK participates in the stabilization and activation of p53 in response to viral infection, which in turn promotes apoptosis before replication of the virus in the host cell. However, this fails to explain a link between TP53RK and the lack of mature IFNAR1 observed in CT26.lacZ, suggesting that possibly both the TP53RK and AKAP7 mutations are acting separately and synergistically to create the ultra sensitive CT26.lacZ phenotype. Our working model proposes that inhibition of IFNAR1 maturation by AKAP7/PKA suppresses intracellular signalling through JAK-STAT, while TP53RK fails to stabilize and activate p53 mediated apoptosis. Taken together these signalling defects would allow for the generation of a population of cells that are highly susceptible to viral infection and viable thus allowing for optimal viral replication.

Conclusion

In conclusion, the original hypothesis stating that CT26.lacZ sensitivity is caused by epigenetic variations affecting the expression of antiviral response genes, was rejected as the major cause for CT26.lacZ sensitivity. While none of the CT26.WT subclones were as sensitive

as CT26.lacZ, the population analysis still demonstrated the surprising amount of heterogeneity that can arise within a cell line, especially considering that CT26.WT are clonally selected themselves. Instead, a new hypothesis supported that the LZSN vector used to transduce the LacZ gene has inserted in the CT26 genome and caused a mutation within a key antiviral response gene or regulatory element. Our findings support the latter and have led to the discovery of two new possible regulators of innate antiviral response. Firstly, AKAP7, a two variant protein that acts a master switch regulator for the JAK-STAT signalling cascade. Secondly, TP53RK, a p53 activating kinase that regulates p53 activation in response to viral stress. While these results are still preliminary, further characterizing the role of these two proteins in modulating viral hypersensitivity and determining their importance to the antiviral response greatly expands our knowledge of viral defence mechanisms and expands our possibilities to develop specific and synergistic therapeutics in the future.

References:

1. Kelly E, Russell SJ. History of oncolytic viruses: Genesis to genetic engineering. *Molecular therapy : the journal of the American Society of Gene Therapy*. 2007;15(4):651-659.
2. Dock G. The influence of complicating diseases upon leukemia. *American Journal of the Medical Sciences*. 1904;127(4):592.

3. Smith W, Andrewes CH, Laidlaw PP. A virus obtained from influenza patients. *The Lancet*. 1933;222(5732):66-68.

4. Pelner L, Fowler G, C H. Effect of concurrent infections and their toxins on the course of leukemia. *Journal of Internal Medicine*. 1958;162(S338):5-24.

5. Bierman HR, Crile DM, Dod KS, et al. Remissions in leukemia of childhood following acute infectious disease: Staphylococcus and streptococcus, varicella, and feline panleukopenia. *Cancer*. 1953;6(3):591-605.

6. Hoster Ha, Zanes RP, Haam EV. The association of "viral" hepatitis and hodgkin ' s disease. *Cancer research*. 1949;7:473-480.

7. Southam CM, Moore aE. Clinical studies of viruses as antineoplastic agents with particular reference to egypt 101 virus. *Cancer*. 1952;5(5):1025-1034.

8. Taylor aW. Effects of glandular fever infection in acute leukaemia. *British medical journal*. 1953;1(4810):589-593.

9. Huber RJ, Bell JA, Rowe WP, et al. Studies of adenoidal-pharyngeal-conjunctival vaccines in volunteers. *Journal of the American Medical Association*. 1955;159(10):986-989.

10. Asada T. Treatment of human cancer with mumps virus. *Cancer*. 1974;34:1907-1928.

11. Le Bœuf F, Batenchuk C, Vähä-Koskela M, et al. Model-based rational design of an oncolytic virus with improved therapeutic potential. *Nature communications*. 2013;4(May): 1974.

12. Viral oncolysate in the management of malignant melanoma. II. clinical studies. 1977;40(2): 680-686.

13. Senzer NN, Kaufman HL, Amatruda T, et al. Phase II clinical trial of a granulocyte-macrophage colony-stimulating factor-encoding, second-generation oncolytic herpesvirus in patients with unresectable metastatic melanoma. *Journal of Clinical Oncology*. 2009;27(34): 5763-5771.

14. Stojdl DF, Lichty B, Knowles S, et al. Exploiting tumor-specific defects in the interferon pathway with a previously unknown oncolytic virus. *Nature medicine*. 2000;6(7):821-825.

15. Cassel Wa, Garrett RE. Newcastle disease virus as an antineoplastic agent. *Cancer*. 1965;18:863-868.

16. Yohn DS, Hammon WM, Atchison RW, Casto BC. Oncolytic potentials of nonhuman viruses for human cancer. II. effects of five viruses on heterotransplantable human tumors. *Journal of the National Cancer Institute*. 1968;41(2):523-529.

17. Ilkow CS, Swift SL, Bell JC, Diallo JS. From scourge to cure: Tumour-selective viral pathogenesis as a new strategy against cancer. *PLoS Pathogens*. 2014;10(1).

18. Errington F, Steele L, Prestwich R, et al. Reovirus activates human dendritic cells to promote innate antitumor immunity. *Journal of immunology (Baltimore, Md. : 1950)*. 2008;180(9): 6018-6026.

19. Breitbach CJ, Paterson JM, Lemay CG, et al. Targeted inflammation during oncolytic virus therapy severely compromises tumor blood flow. *Molecular therapy : the journal of the American Society of Gene Therapy*. 2007;15(9):1686-1693.

20. Lemay CG, Rintoul JL, Kus A, et al. Harnessing oncolytic virus-mediated antitumor immunity in an infected cell vaccine. *Molecular Therapy*. 2012;20(9):1791-1799.

21. Goel A, Carlson SK, Classic KL, et al. Radioiodide imaging and radiovirotherapy of multiple myeloma using VSV(Δ51)-NIS, an attenuated vesicular stomatitis virus encoding the sodium iodide symporter gene. *Blood*. 2007;110(7):2342-2350.

22. Zhao Y, Butler EB, Tan M. Targeting cellular metabolism to improve cancer therapeutics. *Cell death & disease*. 2013;4(3):e532.

23. Mccart JA, Ward JM, Lee J, et al. Systemic cancer therapy with a tumor-selective vaccinia virus mutant lacking thymidine kinase and vaccinia growth factor genes systemic cancer therapy with a tumor-selective vaccinia virus mutant lacking thymidine kinase and vaccinia growth factor genes. 2001:8751-8757.

24. Melnikova VO, Santamaria AB, Bolshakov SV, Ananthaswamy HN. Mutant p53 is constitutively phosphorylated at serine 15 in UV-induced mouse skin tumors: Involvement of ERK1/2 MAP kinase. *Oncogene*. 2003;22(38):5958-5966.

25. Lazo PA, Santos CR. Interference with p53 functions in human viral infections , a target for novel antiviral strategies. 2011(July):285-300.

26. Hummel JL, Safroneeva E, Mossman KL. The role of ICP0-null HSV-1 and interferon signaling defects in the effective treatment of breast adenocarcinoma. *Molecular Therapy*. 2005;12(6):1101-1110.

27. Diallo J, Le Boeuf F, Lai F, et al. A high-throughput pharmacoviral approach identifies novel oncolytic virus sensitizers. *Molecular therapy : the journal of the American Society of Gene Therapy*. 2010;18(6):1123-1129.

28. Shmulevitz M, Marcato P, Lee PWK. Unshackling the links between reovirus oncolysis, ras signaling, translational control and cancer. *Oncogene*. 2005;24(52):7720-7728.

29. Mcnab F, Mayer-barber K, Sher A, Wack A, Garra AO. Type I interferons in infectious disease. *Nature Publishing Group*. 2015;15(2):87-103.

30. Goubau D, Deddouche S, Reis e Sousa C. Cytosolic sensing of viruses. *Immunity*. 2013;38(5):855-869.

31. Pestka S, Krause CD, Walter MR. Interferons, interferon-like cytokines, and their receptors. *Immunological Reviews*. 2004;202:8-32.

32. Runkel L, Pfeffer L, Lewerenz M, et al. Differences in activity between alpha and beta type I interferons explored by mutational analysis. *The Journal of biological chemistry*. 1998;273(14):8003-8008.

33. Takeuchi O, Akira S. Pattern recognition receptors and inflammation. *Cell*. 2010;140(6): 805-820.

34. Hou F, Sun L, Zheng H, Skaug B, Jiang QX, Chen ZJ. MAVS forms functional prion-like aggregates to activate and propagate antiviral innate immune response. *Cell*. 2011;146(3): 448-461.

35. Liu WJ, Wang XJ, Mokhonov VV, Shi P, Randall R, Khromykh Aa. Inhibition of interferon signaling by the new york 99 strain and kunjin subtype of west nile virus involves blockage of STAT1 and STAT2 activation by nonstructural proteins. *Journal of virology*. 2005;79(3): 1934-1942.

36. Yan H, Krishnan K, Greenlund aC, et al. Phosphorylated interferon-alpha receptor 1 subunit (IFNAR1) acts as a docking site for the latent form of the 113 kDa STAT2 protein. *The EMBO journal*. 1996;15(5):1064-1074.

37. Schindler C, Levy DE, Decker T. JAK-STAT signaling: From interferons to cytokines. *Journal of Biological Chemistry*. 2007;282(28):20059-20063.

38. Claudinon J, Gonnord P, Beslard E, et al. Palmitoylation of interferon-α (IFN-α) receptor subunit IFNAR1 is required for the activation of Stat1 and Stat2 by IFN-α. *Journal of Biological Chemistry*. 2009;284(36):24328-24340.

39. Levy DE, Darnell JE. Stats: Transcriptional control and biological impact. *Nature reviews. Molecular cell biology*. 2002;3(9):651-662.

40. Nusinzon I, Horvath CM. Unexpected roles for deacetylation in interferon- and cytokine-induced transcription. *Journal of interferon & cytokine research : the official journal of the International Society for Interferon and Cytokine Research*. 2005;25(12):745-748.

41. Paulson M, Press C, Smith E, Tanese N, Levy DE. IFN-stimulated transcription through a TBP-free acetyltransferase complex escapes viral shutoff. *Nature cell biology*. 2002;4(2): 140-147.

42. Marijanovic Z, Ragimbeau J, Kumar KGS, Fuchs SY, Pellegrini S. TYK2 activity promotes ligand-induced IFNAR1 proteolysis. *The Biochemical journal*. 2006;397(1):31-38.

43. Ivashkiv LB, Donlin LT. Regulation of type I interferon responses. *Nature reviews. Immunology*. 2014;14(1):36-49.

44. Gao S, von der Malsburg A, Paeschke S, et al. Structural basis of oligomerization in the stalk region of dynamin-like MxA. *Nature*. 2010;465(7297):502-506.

45. MacMicking JD. Interferon-inducible effector mechanisms in cell-autonomous immunity. *Nature Reviews Immunology*. 2012;12(5):367-382.

46. Sadler AJ, Williams BRG. Interferon-inducible antiviral effectors. *Nature reviews. Immunology*. 2008;8(7):559-568.

47. Takaoka A, Hayakawa S, Yanai H, et al. Integration of interferon-alpha/beta signalling to p53 responses in tumour suppression and antiviral defence. *Nature*. 2003;424(6948):516-523.

48. Kaufman HL, Kim DW, DeRaffele G, Mitcham J, Coffin RS, Kim-Schulze S. Local and distant immunity induced by intralesional vaccination with an oncolytic herpes virus encoding GM-CSF in patients with stage IIIc and IV melanoma. *Annals of surgical oncology*.

2010;17(3):718-730.

49. Senzer NN, Kaufman HL, Amatruda T, et al. Phase II clinical trial of a granulocyte-macrophage colony-stimulating factor-encoding, second-generation oncolytic herpesvirus in patients with unresectable metastatic melanoma. *Journal of Clinical Oncology*. 2009;27(34): 5763-5771.

50. Benboudjema L, Mulvey M, Gao Y, Pimplikar SW, Mohr I. Association of the herpes simplex virus type 1 Us11 gene product with the cellular kinesin light-chain-related protein PAT1 results in the redistribution of both polypeptides. *Journal of virology*. 2003;77(17): 9192-9203.

51. Colamonici OR, Domanski P, Sweitzer SM, Larner a, Buller RML. Vaccinia virus B18R gene encodes a type I interferon-binding protein that blocks interferon ß transmembrane signaling. *Journal of Biological Chemistry*. 1995;270(27):15974-15978.

52. Cronin M, Le Boeuf F, Murphy C, et al. Bacterial-mediated knockdown of tumor resistance to an oncolytic virus enhances therapy. *Molecular therapy : the journal of the American Society of Gene Therapy*. 2014;22(6):1-10.

53. Alcamí a, Symons Ja, Smith GL. The vaccinia virus soluble alpha/beta interferon (IFN) receptor binds to the cell surface and protects cells from the antiviral effects of IFN. *Journal of virology*. 2000;74(23):11230-11239.

54. Vähä-Koskela MJV, Kallio JP, Jansson LC, et al. Oncolytic capacity of attenuated replicative semliki forest virus in human melanoma xenografts in severe combined immunodeficient mice. *Cancer Research*. 2006;66(14):7185-7194.

55. Letchworth GJ, Rodriguez LL, Del cbarrera J. Vesicular stomatitis. *Veterinary journal (London, England : 1997)*. 1999;157(3):239-260.

56. Iverson LE, Rose JK. Localized attenuation and discontinuous synthesis during vesicular stomatitis virus transcription. *Cell*. 1981;23(2):477-484.

57. Barr JN, Whelan SP, Wertz GW. Role of the intergenic dinucleotide in vesicular stomatitis virus RNA transcription. *Journal of virology*. 1997;71(3):1794-1801.

58. Finkelshtein D, Werman A, Novick D, Barak S, Rubinstein M. LDL receptor and its family members serve as the cellular receptors for vesicular stomatitis virus. *Proceedings of the National Academy of Sciences of the United States of America*. 2013;110(18):7306-11.

59. Schlegel R, Wade M. Neutralized vesicular stomatitis virus binds to host cells by a different "receptor". *Biochemical and biophysical research communications*. 1983;114(2):774-778.

60. Superti F, Seganti L, Ruggeri FM, Tinari a, Donelli G, Orsi N. Entry pathway of vesicular stomatitis virus into different host cells. *The Journal of general virology*. 1987;68 (Pt 2): 387-399.

61. Lichty BD, Power AT, Stojdl DF, Bell JC. Vesicular stomatitis virus: Re-inventing the bullet. *Trends in Molecular Medicine*. 2004;10(5):210-216.

62. Puri a, Krumbiegel M, Dimitrov D, Blumenthal R. A new approach to measure fusion

activity of cloned viral envelope proteins: Fluorescence dequenching of octadecylrhodamine-labeled plasma membrane vesicles fusing with cells expressing vesicular stomatitis virus glycoprotein. *Virology*. 1993;195(2):855-858.

63. Fredericksen BL, Whitt Ma. Vesicular stomatitis virus glycoprotein mutations that affect membrane fusion activity and abolish virus infectivity. *Journal of virology*. 1995;69(3): 1435-1443.

64. Her LS, Lund E, Dahlberg JE. Inhibition of ran guanosine triphosphatase-dependent nuclear transport by the matrix protein of vesicular stomatitis virus. *Science (New York, N.Y.)*. 1997;276(5320):1845-1848.

65. Stojdl DF, Lichty BD, tenOever BR, et al. VSV strains with defects in their ability to shutdown innate immunity are potent systemic anti-cancer agents. *Cancer Cell*. 2003;4(4): 263-275.

66. Parato K, Breitbach CJ, Le Boeuf F, et al. The oncolytic poxvirus JX-594 selectively replicates in and destroys cancer cells driven by genetic pathways commonly activated in cancers. *Molecular Therapy*. 2012;20(4):749-758.

67. Saloura V, Wang LS, Fridlender ZG, et al. Evaluation of an attenuated vesicular stomatitis virus vector expressing interferon-beta for use in malignant pleural mesothelioma: Heterogeneity in interferon responsiveness defines potential efficacy. *Human gene therapy*. 2010;21(1):51-64.

68. Hadaschik B, Zhang K, So AI, et al. Oncolytic vesicular stomatitis viruses are potent agents for intravesical treatment of high-risk bladder cancer. *Cancer Research*. 2008;68(12): 4506-4510.

69. Murayama A, Sugiyama N, Yoshimura S, et al. A subclone of HuH-7 with enhanced intracellular hepatitis C virus production and evasion of virus related-cell cycle arrest. *PLoS ONE*. 2012;7(12):1-9.

70. Ruotsalainen JJ, Kaikkonen MU, Niittykoski M, et al. Clonal variation in interferon response determines the outcome of oncolytic virotherapy in mouse CT26 colon carcinoma model. . 2014(August 2014):65-75.

71. Wang M, Bronte V, Chen PW, et al. Active immunotherapy of cancer with a nonreplicating recombinant fowlpox virus encoding a model tumor-associated antigen. *Journal of immunology (Baltimore, Md. : 1950)*. 1995;154(9):4685-4692.

72. Miller aD, Rosman GJ. Improved retroviral vectors for gene transfer and expression. *BioTechniques*. 1989;7(9):980-990.

73. Puzanov I, Milhem M, Andtbacka R, et al. Primary analysis of a phase 1b multicenter trial to evaluate safety and efficacy of talimogene laherparepvec (T-VEC) and ipilimumab (ipi) in previously untreated, unresected stage IIIB-IV melanoma. *Journal of Clinical Oncology*. 2014;32(15):supplemental.

74. Heo J, Reid T, Ruo L. Randomized dose-finding clinical trial of oncolytic immunotherapeutic vaccinia JX-594 in liver cancer. *Nature Medicine*. 2013;15(5):242.

75. Brun J, McManus D, Lefebvre C, et al. Identification of genetically modified maraba virus as an oncolytic rhabdovirus. *Molecular therapy : the journal of the American Society of Gene Therapy*. 2010;18(8):1440-1449.

76. Sakamoto S, Potla R, Larner AC. Histone deacetylase activity is required to recruit RNA polymerase II to the promoters of selected interferon-stimulated early response genes. *Journal of Biological Chemistry*. 2004;279:40362-40367.

77. Schindler C, Levy DE, Decker T. JAK-STAT signaling: From interferons to cytokines. *Journal of Biological Chemistry*. 2007;282(28):20059-20063.

78. Burrell Ra, McGranahan N, Bartek J, Swanton C. The causes and consequences of genetic heterogeneity in cancer evolution. *Nature*. 2013;501(7467):338-45.

79. Hatzivassiliou G, Song K, Yen I, et al. RAF inhibitors prime wild-type RAF to activate the MAPK pathway and enhance growth. *Nature*. 2010;464(7287):431-435.

80. Poulikakos PI, Persaud Y, Janakiraman M, et al. RAF inhibitor resistance is mediated by dimerization of aberrantly spliced BRAF(V600E). *Nature*. 2011;480(7377):387-390.

81. Smallwood Sa, Lee HJ, Angermueller C, et al. Single-cell genome-wide bisulfite sequencing for assessing epigenetic heterogeneity. *Nature Methods*. 2014;11(8):817-20.

82. Wang Y, Li X, Hu H. H3K4me2 reliably defines transcription factor binding regions in different cells. *Genomics*. 2014;103(2-3):222-8.

83. Park PJ. ChIP-seq: Advantages and challenges of a maturing technology. *Nature reviews. Genetics*. 2009;10(10):669-680.

84. Huck-Hui N, Bird a. DNA methylation and chromatin modification. *Current Opinion in Genetics and Development*. 1999;9(2):158-163.

85. Cowper-Sal·lari R, Zhang X, Wright JB, et al. Breast cancer risk–associated SNPs modulate the affinity of chromatin for FOXA1 and alter gene expression. *Nature Genetics*. 2012;44(11): 1191-1198.

86. Quackenbush J. Microarray data normalization and transformation. . 2002;32(december): 496-501.

87. Irizarry Ra, Hobbs B, Collin F, et al. Exploration, normalization, and summaries of high density oligonucleotide array probe level data. *Biostatistics (Oxford, England)*. 2003;4(2): 249-264.

88. Bolstad BM, Bolstad BM, Irizarry Ra, et al. A comparison of normalization metholds for high density oligonucleotide array data based on variance and bias. *Bioinformatics*. 2003;19(2):185-193.

89. Adams CP, Kron SJ. Method for performing amplification of nucleic acid with two primers bound to a single solid support. . 1997.

90. Zhang Y, Liu T, Meyer Ca, et al. Model-based analysis of ChIP-seq (MACS). *Genome biology*. 2008;9(9):R137.

91. Ernst J, Kellis M. Discovery and characterization of chromatin states for systematic annotation of the human genome. *Nature biotechnology*. 2010;28(8):817-825.

92. Ernst J, Kellis M. ChromHMM: Automating chromatin-state discovery and characterization. *Nature Methods*. 2012;9(3):215-216.

93. Zhang Y, Shin H, Song JS, Lei Y, Liu XS. Identifying positioned nucleosomes with epigenetic marks in human from ChIP-seq. *BMC genomics*. 2008;9:537.

94. He HH, Meyer Ca, Shin H, et al. Nucleosome dynamics define transcriptional enhancers. *Nature genetics*. 2010;42(4):343-347.

95. Liu T, Ortiz Ja, Taing L, et al. Cistrome: An integrative platform for transcriptional regulation studies. *Genome Biology*. 2011;12(8):R83.

96. Carvalho BS, Irizarry Ra. A framework for oligonucleotide microarray preprocessing. *Bioinformatics*. 2010;26(19):2363-2367.

97. Eden E, Navon R, Steinfeld I, Lipson D, Yakhini Z. GOrilla: A tool for discovery and visualization of enriched GO terms in ranked gene lists. *BMC bioinformatics*. 2009;10:48.

98. Eden E, Lipson D, Yogev S, Yakhini Z. Discovering motifs in ranked lists of DNA sequences. *PLoS Computational Biology*. 2007;3(3):508.

99. Supek F, Bošnjak M, Škunca N, Šmuc T. Revigo summarizes and visualizes long lists of gene ontology terms. *PLoS ONE*. 2011;6(7).

100. Garcia V, Krishnan R, Davis C, et al. High-throughput titration of luciferase-expressing recombinant viruses 3 . preparation of viral standard curve. *Journal of Visual Biology*. 2014;91(September):1-8.

101. Garcia V, Krishnan R, Davis C, et al. High-throughput titration of luciferase-expressing recombinant viruses video link. *J. Vis. Exp*. 2014(10):518903791-51890.

102. Gold MG, Fowler DM, Means CK, et al. Engineering A-kinase anchoring protein (AKAP)-selective regulatory subunits of protein kinase A (PKA) through structure-based phage selection. *Journal of Biological Chemistry*. 2013;288(24):17111-17121.

103. Jones BW, Brunet S, Gilbert ML, et al. Cardiomyocytes from AKAP7 knockout mice respond normally to adrenergic stimulation. *Proceedings of the National Academy of Sciences*. 2012;109(42):17099-17104.

104. Ling LE, Zafari M, Reardon D, Brickelmeier M, Goelz SE, Benjamin CD. Human type I interferon receptor, IFNAR, is a heavily glycosylated 120-130 kD membrane protein. *Journal of interferon & cytokine research : the official journal of the International Society for Interferon and Cytokine Research*. 1995;15(1):55-61.

105. Tai Z, Lin Y, He Y, et al. Luteolin sensitizes the antiproliferative effect of interferon α/ß by activation of janus kinase/signal transducer and activator of transcription pathway signaling through protein kinase A-mediated inhibition of protein tyrosine phosphatase SHP-2 in can. *Cellular Signalling*. 2014;26(3):619-628.

106. Lee EH, Rikihisa Y. Protein kinase A-mediated inhibition of gamma interferon-induced

tyrosine phosphorylation of janus kinases and latent cytoplasmic transcription factors in human monocytes by ehrlichia chaffeensis. *Infection and Immunity*. 1998;66(6):2514-2520.

107. Kawada N, Uoya M, Seki S, Kuroki T, Kobayashi K. Regulation by cAMP of STAT1 activation in hepatic stellate cells. *Biochemical and biophysical research communications*. 1997;233(2):464-469.

108. Pace TWW, Hu F, Miller AH. Activation of cAMP-protein kinase A abrogates STAT5-mediated inhibition of glucocorticoid receptor signaling by interferon-alpha. *Brain, Behavior, and Immunity*. 2011;25(8):1716-1724.

109. David M, Petricoin E, Larner AC. Activation of protein kinase A inhibits interferon induction of the jak/stat pathway in U266 cells. *Journal of Biological Chemistry*. 1996;271(9): 4585-4588.

110. Brown RL, August SL, Williams CJ, Moss SB. AKAP7γ is a nuclear RI-binding AKAP. *Biochemical and Biophysical Research Communications*. 2003;306(2):394-401.

111. Abe Y, Matsumoto S, Wei S, et al. Cloning and characterization of a p53-related protein kinase expressed in interleukin-2-activated cytotoxic T-cells, epithelial tumor cell lines, and the testes. *Journal of Biological Chemistry*. 2001;276(47):44003-44011.

112. Abe Y, Takeuchi T, Imai Y, et al. A small ras-like protein ray/Rab1c modulates the p53-regulating activity of PRPK. *Biochemical and Biophysical Research Communications*. 2006;344(1):377-385.

113. Garijo R, Hernández-Alonso P, Rivas C, Diallo JS, Sanjuán R. Experimental evolution of an oncolytic vesicular stomatitis virus with increased selectivity for p53-deficient cells. *PLoS ONE*. 2014;9(7):1-8.

114. Teufel DP, Bycroft M, Fersht aR. Regulation by phosphorylation of the relative affinities of the N-terminal transactivation domains of p53 for p300 domains and Mdm2. *Oncogene*. 2009;28(20):2112-2118.

Contributors and Collaborators

Dr. Lupiens lab at the Princess Margaret Cancer Center/University Health Network in Toronto performed the chromatin immunoprecipitation and sequencing of CT26.WT and CT26.lacZ for this study. The analysis (ChromHMM and SeqPos) was performed on the computer clusters in

Toronto by Parisa Mazrooei as we were unable to run this size of data on our system. Dr. Mathieu Lupien's team were great at passing on their expertise and teaching me tools and tips from their extensive knowledge of epigenetic analysis.

Dr. Fabrice Leboeuf infected and sent the CT26 samples for the microarray data used in this Thesis.

Appendix

Allele	CT26.WT Size	CT26.lacZ Size
18-3	19	19
4-2	21.3	21.3
6-7	12	12
9-2	15	15
15-3	21.3	22.3
6-4	17	19
12-1	16	17
5-5	14	14
X-1	25	26

Supplemental 1: Short tandem repeat analysis of CT26.WT and CT26.lacZ confirms that these CT26.lacZ derive from the CT26.WT used and that there is no contamination in the cultures.

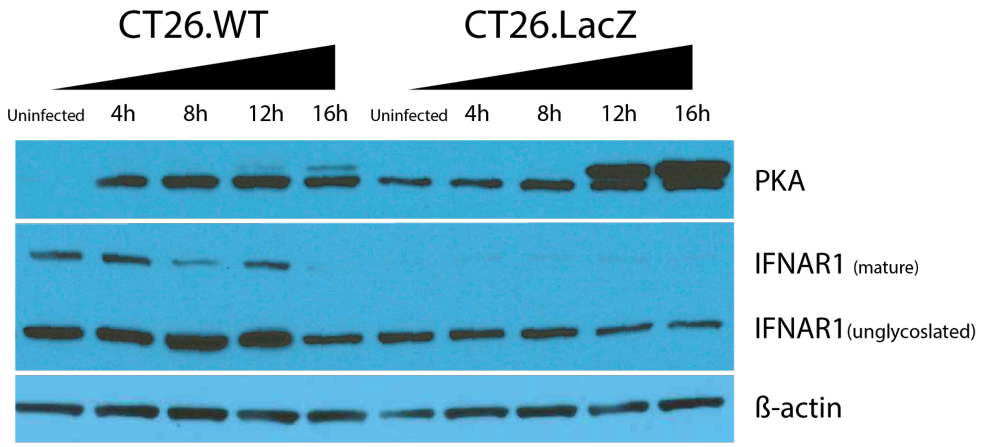

Supplemental 2: Inverse relationship with PKA and mature IFNAR1 in CT26.WT. In CT26.lacZ PKA is persistently highly expressed and there is no mature IFNAR1.